A Computational Model of the Ionic Currents, Ca^{2+} Dynamics and Action Potentials Underlying Contraction of Isolated Uterine Smooth Muscle

Wing-Chiu Tong[1,2], Cecilia Y. Choi[3], Sanjay Karche[3], Arun V. Holden[4], Henggui Zhang[3]*, Michael J. Taggart[1,2]*

1 Institute of Cellular Medicine, Newcastle University, Newcastle upon Tyne, United Kingdom, 2 Maternal and Fetal Health Research Centre, St. Mary's Hospital, University of Manchester, Manchester, United Kingdom, 3 School of Physics and Astronomy, University of Manchester, Manchester, United Kingdom, 4 Institute of Membrane and System Biology, University of Leeds, Leeds, United Kingdom

Abstract

Uterine contractions during labor are discretely regulated by rhythmic action potentials (AP) of varying duration and form that serve to determine calcium-dependent force production. We have employed a computational biology approach to develop a fuller understanding of the complexity of excitation-contraction (E-C) coupling of uterine smooth muscle cells (USMC). Our overall aim is to establish a mathematical platform of sufficient biophysical detail to quantitatively describe known uterine E-C coupling parameters and thereby inform future empirical investigations of physiological and pathophysiological mechanisms governing normal and dysfunctional labors. From published and unpublished data we construct mathematical models for fourteen ionic currents of USMCs: Ca^{2+} currents (L- and T-type), Na^{+} current, an hyperpolarization-activated current, three voltage-gated K^{+} currents, two Ca^{2+}-activated K^{+} current, Ca^{2+}-activated Cl current, non-specific cation current, Na^{+}-Ca^{2+} exchanger, Na^{+}-K^{+} pump and background current. The magnitudes and kinetics of each current system in a spindle shaped single cell with a specified surface area:volume ratio is described by differential equations, in terms of maximal conductances, electrochemical gradient, voltage-dependent activation/inactivation gating variables and temporal changes in intracellular Ca^{2+} computed from known Ca^{2+} fluxes. These quantifications are validated by the reconstruction of the individual experimental ionic currents obtained under voltage-clamp. Phasic contraction is modeled in relation to the time constant of changing $[Ca^{2+}]_i$. This integrated model is validated by its reconstruction of the different USMC AP configurations (spikes, plateau and bursts of spikes), the change from bursting to plateau type AP produced by estradiol and of simultaneous experimental recordings of spontaneous AP, $[Ca^{2+}]_i$ and phasic force. In summary, our advanced mathematical model provides a powerful tool to investigate the physiological ionic mechanisms underlying the genesis of uterine electrical E-C coupling of labor and parturition. This will furnish the evolution of descriptive and predictive quantitative models of myometrial electrogenesis at the whole cell and tissue levels.

Introduction

For over 50 years it has been known that uterine smooth muscle (myometrium) generates spontaneous action potentials (APs) [1–3]. These precede elevations in intracellular Ca^{2+} that, in turn, facilitate the actomyosin interactions governing myometrial contractions [4,5]. The regulation of electrical activity of myometrial cells therefore plays a crucial role in determining the onset, the duration and the strength of uterine contractions during labor. This is essential for a successful conclusion to pregnancy with the safe delivery of the fetus and placenta. Unfortunately, many pregnancies result in complications of labor that compromise the health of the fetus/newborn. Preterm birth, of which activation of uterine contraction is the major cause, occurs in up to 12% of deliveries and results in a high incidence of mortality and morbidity of the offspring [6]. Prolonged dysfunctional labor at term occurs in 10% of pregnancies and these patients account for 20% of Cesarean sections [7]. An improved understanding of the physiological complexities of myometrial electrical excitability would assist in the task of developing better targeted therapies for these problematic labors.

Modifications of myometrial cell electrophysiological characteristics during pregnancy are evident. The resting membrane potential of myometrial cells becomes progressively more positive towards term [8], gestational-dependent changes in the molecular expressions of ionic channel components occurs [9] and the form of action potentials can change between those of rapid spike-like and tonic plateau-type [10,11]. Electrophysiological recordings have also identified several classes of individual ionic currents in myometrial cells. It is accepted that the major inward depolarizing

current of the AP likely arises from Ca^{2+} entry via L-type Ca^{2+} channels [12]. Other myometrial inward currents that have been suggested to be functional, at least in some experimental situations, include those mediated through T-type Ca^{2+} channels [13], Na^+ channels [14] or Cl^- channels [15]. Voltage-dependent outward currents, both those that are sensitive or insensitive to 4-aminopyridine (4-AP), have been identified as have calcium-dependent K^+ currents [16–20]. Molecular expression of genes/proteins of electrogenic ion exchangers, the Na^+-K^+ ATPase [21] and the Na^+-Ca^{2+} exchangers [22], suggest that these too may have a contribution to make to regulating myometrial membrane potential.

There is increasing awareness of the benefits of developing mathematical descriptions of uterine function [23–25] and recent attempts have shown promise regarding the mapping of electrophysiological or contractile data. However, detailed descriptions of the biophysical characteristics of each of the myometrial ionic currents are lacking. In addition, information on how these individual ionic currents are integrated to form the shape and timecourse of APs reflective of those reported for the myometrium is sparse. This severely limits the ability to model simultaneous changes in myometrial membrane potential, $[Ca^{2+}]_i$ and force that are the essential elements of electrical E-C coupling. It is important to determine each of these circumstances in order to assess fully the likely physiological relevance to AP genesis of any electrophysiological data that has been recorded in isolation and attributed to a particular ion channel subtype. It is also necessary to consider how these electrical events influence E-C coupling parameters leading to the generation of phasic contractions of uterine smooth muscle as this, after all, determines the success of the parturient effort. Therefore, we had three aims to the present work. First, to develop biophysically detailed quantitative (mathematical) descriptions of all known individual ionic currents of uterine smooth muscle cells pertaining to near the end of pregnancy. Second, to compute these, in alliance with descriptions of dynamic Ca^{2+} handling parameters, into a mathematical model of myometrial action potential generation. Third, to extend this model to the simulation of concomitant recordings of spontaneous AP, Ca^{2+} and force in uterine smooth muscle. Moreover, the model is assessed for its ability to simulate published changes in experimental parameters. The development of our quantitative model markedly advances our understanding of the electrophysiological basis of excitation-contraction coupling in uterine smooth muscle. In so doing, it also provides a framework of relevance for exploring the biophysical modeling of individual ionic currents underlying the electrogenic processes in other smooth muscles, tissues and organs.

Results and Discussion

The general mathematical formulae used for parameter modeling are given in the Methods (equations 1–9). A glossary of symbols used in the modeling equations is given in Tables S1, S2. Detailed formulations of individual model components are given in Appendix S1 (equations 10–105).

L-type Calcium current – I_{CaL}

Mathematical descriptions of the biophysical characteristics of this current are given in Appendix S1 (equations 10–19).

I_{CaL} is attributed as the major inward current in myometrial cells [8,14,26–28]. I_{CaL} first appears at $V \approx -40$ to -30 mV; the peak of the current-voltage (I–V) relationship arises between $V = -10$ to 10 mV and the reversal potential $E_{CaL} \approx 45$ to 60 mV at $30-35°C$ with $1.5-2.5$ mM $[Ca^{2+}]_o$ [12,15,29,30]. L-type calcium channels in other cell types have been reported to be

permeable to other cations [31] but there is no data specific to myometrial cells. Thus, the Goldman-Hodgkin-Katz formulation commonly used in other muscle cell models is not used here; instead, E_{CaL} in the model is fixed at 45 mV as suggested by experimental data [12,30,32].

Properties of I_{CaL} are derived from experimental data at $30-35°C$ of myometrial cells from late pregnant rat. The equations of I_{CaL} incorporate an activation gating variable (d) and fast (f_1) and slow (f_2) inactivation gating variables. Different steady-state values for activation and inactivation at $30-35°C$ have been reported and representatives of the data range are plotted in Figure 1A–B. This may reflect different $[Ca^{2+}]_o$ employed between studies or slightly differing residual hormonal influences. Yoshino et al., [33] showed that the half-activation and the I–V relationship were right-shifted by ≈ 15 mV when $[Ca^{2+}]_o$ was increased from 3 mM to 30 mM; the rather rightward steady-state inactivation values from Amedee et al., [29] were recorded from myometrial cells exposed to 10 mM $[Ca^{2+}]_o$. Yamamoto [30] showed that the I_{CaL} half-inactivation was left-shifted, and the I–V relationship was reduced, in the myometrial cells exposed to estradiol; in rodents, estradiol increases near term. The myometrial cells from late pregnant rats reported by Shmigol et al., [12] exhibit a leftward shift in inactivation and activation curves relative to the other reports possibly reflective of an influence of altered steroidal levels near term. Alternatively, as the holding potential (V_h) in Shmigol et al., [12] was -80 mV, a tentative explanation could be the additional presence of I_{CaT} (see below) contributing to this dataset. In the model, we placed the I_{CaL} steady-state functions close to the control datasets from Yamamoto [30], which are representative of the steady-state values of I_{CaL} from a collection of other studies that, for clarity of presentation, are not plotted in Figure 1 [14,33–35].

There is little information available for voltage-dependent activation time constants of myometrial I_{CaL}, so we proceeded to extract time constants from published I_{CaL} current tracings. Amedee et al., [29] and Jones et al., [15] had reported I_{CaL} current tracings at $30-35°C$, but in Amedee et al., [29] only at a single voltage step and of poor quality for curve fitting purposes. There are other I_{CaL} current tracings [14,33–35] at room temperature but we are unaware of published Q_{10} values for myometrial I_{CaL}. The experiments of Jones et al., [15], performed at $35°C$, were designed to study $I_{Cl(Ca)}$ wherein I_{CaL} was first activated to enable plasmalemmal Ca^{2+} entry that, subsequently, activated a current taken to be $I_{Cl(Ca)}$. The initial fast inward current was attributed as I_{CaL} because it was blocked by nifedipine, was permeable to Ba^{2+} and was increased by the L-type Ca channel agonist Bay K8644. We presumed that activation of $I_{Cl(Ca)}$ would be slower than I_{CaL} and, thus, voltage-dependent activation time constants for I_{CaL} were obtained by fitting the initial few tens of milliseconds of raw data tracings, *i.e.* prior to peak current at each voltage step being reached, from Jones et al., [15] (Figure 1C). This assumption is backed up by the activation time constants for I_{CaL} in other smooth muscles being $2-8$ ms whereas that for $I_{Cl(Ca)}$ has been estimated at >50 ms [36]. The two inactivation time constants, f_1 and f_2, were taken from Amedee et al., [29] (Figure 1D). The fast inactivation f_1 is voltage-independent at ≈ 12 ms and the slow inactivation is voltage-dependent with a minimum of ≈ 55 ms at $V = 0$ mV.

Simulated time tracings of I_{CaL} under voltage-clamp conditions and I_{CaL} I–V relationships were compared to experimental data in Figure 1E–F. The simulated time tracings closely matched the experimental time data from Jones et al., [15]; I_{CaL} reached its peak in ≈ 12 ms then quickly inactivated. Only the time tracings at voltage steps between $-40-0$ mV from Jones et al., [15] were used for comparison in order to minimize contamination by $I_{Cl(Ca)}$. The
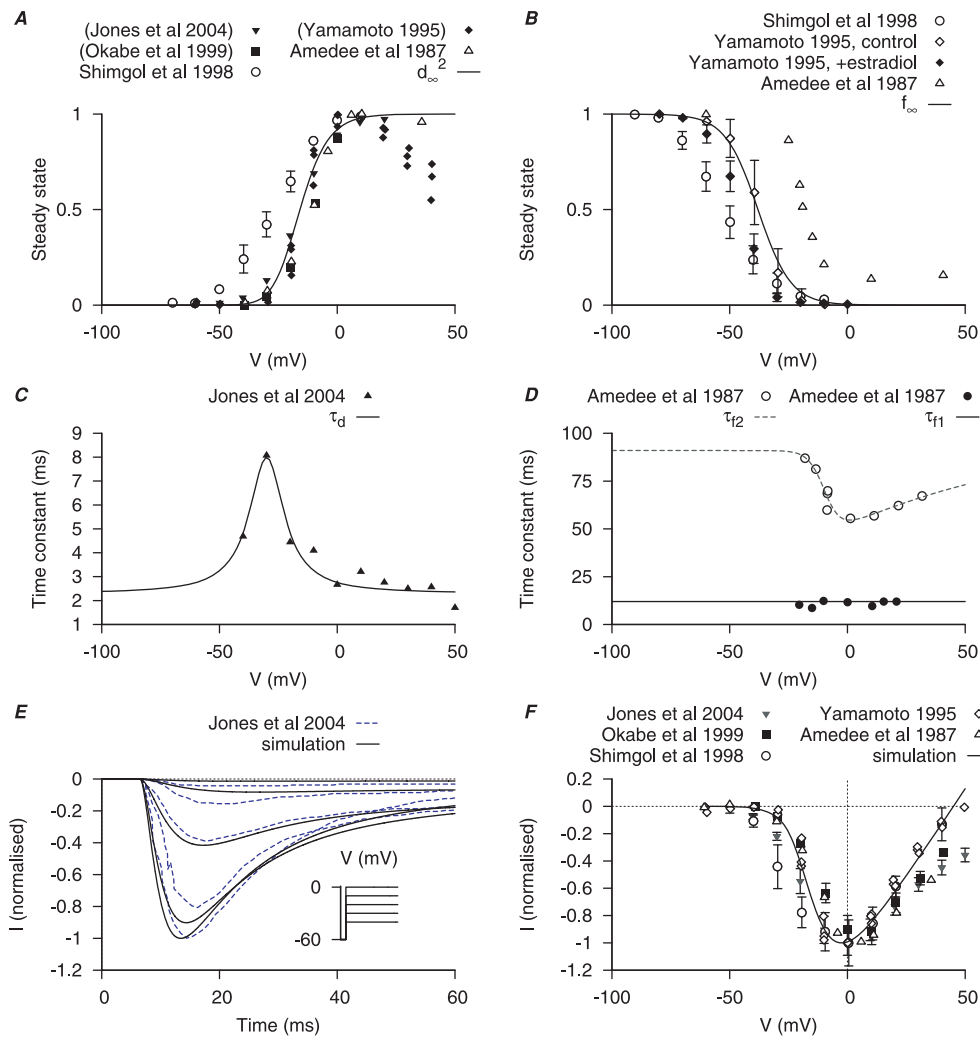
Figure 1. Myometrial I_{CaL} model. Properties of I_{CaL} are derived from experimental data of myometrial longitudinal cells from late pregnant rat [12,15,29,30,32,35]. *A*, voltage (V)-dependent activation steady-state ($d_\infty{}^2$); experimental data in brackets were extrapolated from current-voltage (I–V) relationships using the function $d_\infty{}^2(V) = I_{CaL}/(V - E_{CaL})$ and normalized to the maximum value. *B*, V-dependent inactivation steady-state (f_∞). *C*, V-dependent activation time constant (τ_d); extracted by fitting current tracings from Jones *et al.* [15]. *D*, V-independent fast inactivation time constant (τ_{f1}, *solid circles*) and V-dependent slow inactivation time constant (τ_{f2}, *empty circles*). *E*, simulated voltage-clamp I_{CaL} at voltage steps of -40 to $0\,mV$ from a holding potential of $-60\,mV$ are superimposed on experimental current tracings from Jones *et al.*, [15]; *F*, simulated peak I–V relationship of I_{CaL} together with different experimental I–V data. In both *E* and *F*, all data are normalized to the peak current value at $V = 0\,mV$.
doi:10.1371/journal.pone.0018685.g001

simulated I–V relationship further shows that I_{CaL} first appears at $V \approx -40 - -30\,mV$ and peaks at $V = 0\,mV$, similar to that seen experimentally [12,15,29,30]. Validation of the model is also evinced by the ability to reproduce the effects of estradiol on the I_{CaL} I–V relationships reported by Yamamoto [30]. Herein, the effect on the simulated I–V relationship of experimentally observed estradiol-induced changes in current were examined. The model reproduced the estradiol-mediated leftward shift in inactivation, and the reduction in I–V amplitude, from a V_h of $-40\,mV$ (Figure S1).

Peak I_{CaL} currents in myometrial cells of late pregnant rat have been reported to be $\approx -6.62 \pm 0.55\,pA\,pF^{-1}$ ($V_h = -60\,mV$, Jones *et al.*, [15]) and $\approx -5.23 \pm 0.6\,pA\,pF^{-1}$ ($V_h = -50\,mV$, Okabe *et al.*, [32]) at $30 - 35°C$. This gives a maximal conductance ($\bar{g}_{CaL}$) of $\approx 0.35\,nS\,pF^{-1}$ for modeling the ionic current data.

With $\bar{g}_{CaL} = 0.35\,nS\,pF^{-1}$ in the later development of the USMC action potential simulations, the rate of rise of an AP was $\approx 2.5\,V\,s^{-1}$ which was less than the reported experimental range

of $5 - 10\,V\,s^{-1}$ [37]. Thus, it is necessary to set $\bar{g}_{CaL}$ at a higher value at $0.6\,nS\,pF^{-1}$.

It is possible that the reported I_{CaL} current density may represent the lower limits in late pregnant rat myometrial cells given that (i) the expression of mRNA encoding L-type Ca channel protein subunits increases before labor in rat myometrial cells [38–40] and the protein expression of the pore forming $\alpha 1C$ subunit is regulated by ratio of sex hormones [41]; (ii) the I_{CaL} current density may be underestimated by *in vitro* experimental conditions: I_{CaL} current density in isolated cells diminishes with time [11,15]. Myometrial I_{CaL} also showed calcium-dependent inactivation [26,29]. This is described by a Hill equation with $K_{m,Ca} = 1\,mM$ and a Hill coefficient of 4 in the whole USMC cell model.

Sodium current – I_{Na}

Mathematical descriptions of the biophysical characteristics of this current are given in Appendix S1 (equations 20–27).

Modeling of I_{Na} is accomplished using data from myometrial cells of late pregnant rats or humans recorded at room temperature [14,33,34,42]. I_{Na} first appears at $V \approx -50\,mV$ and the peak I–V relationship occurs between $V = -10$ to $+10\,mV$. Raw data current tracings showed that I_{Na} reached its peak of activation within $\approx 1\,ms$ and almost completely inactivated after $10-20\,ms$ [14,33,34,42].

The equation for I_{Na} incorporates an activation gating variable (m) and an inactivation gating variable (h). Steady-state values for activation and inactivation are shown in Figure 2A. The time constants of activation and inactivation (Figure 2B) were each obtained by fitting the raw data current tracings from the literature [14,33,34,42]. Simulated traces of I_{Na} current under voltage-clamp conditions presented in Figure 2C show dynamic profiles similar to the raw data [14,33,34,42]: at voltage steps of $-40\,mV$ to $0\,mV$, from a V_h of $-90\,mV$, I_{Na} reached its peak in $\approx 2\,ms$ then quickly inactivated within $10\,ms$. The reported peak currents for I_{Na} range from -0.86 to $-3.67\,pA\,pF^{-1}$ [33,34,42], which gives a maximal conductance range $\bar{g}_{Na}$ of $\approx 0.028-0.125\,nS\,pF^{-1}$. Simulated I–V relationship of I_{Na} matched to the experimental data as shown in Figure 2D [14,34,42].

T-type Calcium current – I_{CaT}

Mathematical description of the biophysical characteristics of this current are given in Appendix S1 (equations 28–34).

I_{CaT} has been reported in human myometrial cells [13,14,28,37,42]. Moreover: (i) Ohkubo et al., [40] showed that the expressions of mRNA encoding for the α1G and α1H protein subunits of the T-type calcium channel were gestationally regulated in rat myometrial cells; (ii) detailed electrophysiological data of cells expressing rat α1G/Cav3.1 are available [43,44]; and (iii) spontaneous contractions in myometrial tissue strips from late

pregnant rats were markedly inhibited by the putative T-type calcium channel blockers mibefradil, NNC 55-0396 (a non-hydrolyzable analogue of mibefradil) and Ni^+ [45,46]. Therefore, we developed a model of I_{CaT} electrophysiological characteristics from the rat α1G/Cav3.1 clonal expression cell data recorded at room temperature [43,44] adjusted to the current density of human myometrial cell I_{CaT} [13,18,28]. It is note-worthy that the activation and inactivation steady-state values, and the I–V relationships, are similar between these different datasets.

I_{CaT} first appears at $V \approx -60\,mV$, the peak I–V relationship occurs between $-20\,mV$ and $-30\,mV$, and published raw data current tracings indicate a fast activation but with inactivation temporal profiles varying between $7-100\,ms$ [13,18,28,43,44,47] Figure S2. This last may be influenced by the different external divalent cation concentrations used between experimental conditions (Figure S3). The datasets with the fastest inactivation profiles expected of I_{CaT} had the highest divalent cation concentrations and, indeed, were those attributed to Serrano et al., [43], Hering et al., [44] and Blanks et al., [13].

The equation for I_{CaT} incorporates an activation gating variable (b) and an inactivation gating variable (g). Steady-state values for activation and inactivation are shown in Figure 3A. A function is chosen for activation time constants to fit the time-to-peak experimental data (Figure 3B). The time constant of inactivation is shown in Figure 3C. Simulated I_{CaT} tracings under voltage-clamp conditions and I–V relationships are shown in Figure 3D and Figure 3E respectively and are compared to experimental data from Serrano et al., [43] and Hering et al., [44]. In Figure 3E, E_{CaT} is fixed at $25\,mV$ to match the experimental values in Serrano et al., [43] and Hering et al., [44]. The reported peak current for I_{CaT} is $\approx -1.5\,pA\,pF^{-1}$ at $V = -30\,mV$ from a V_h of $-80\,mV$
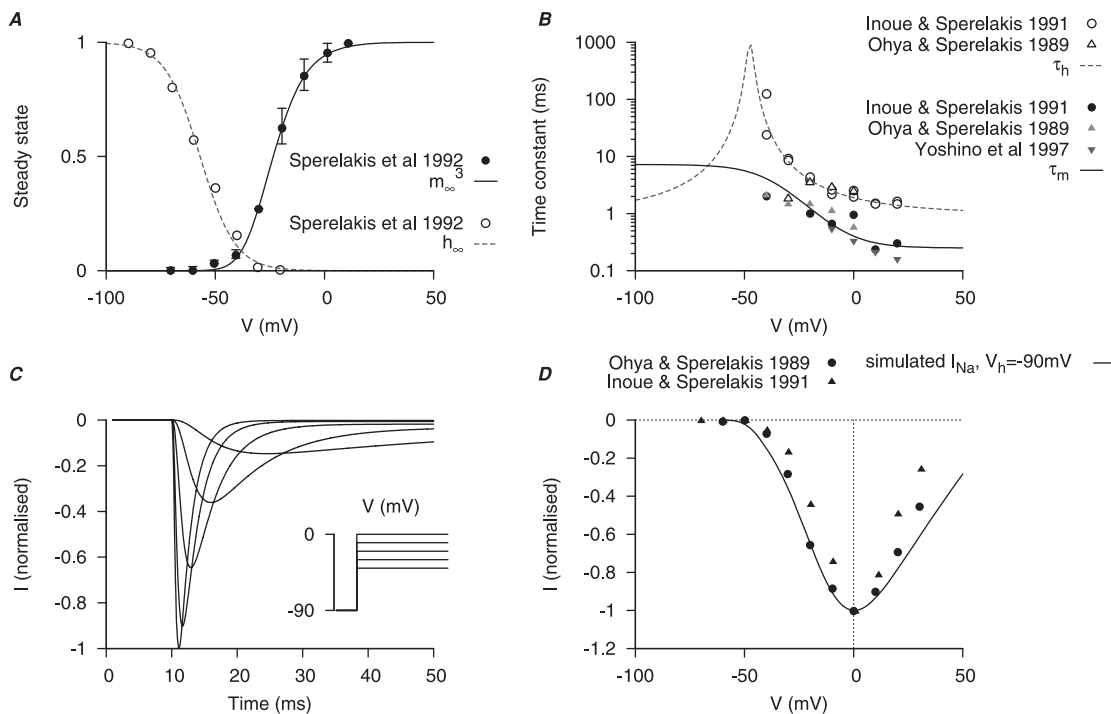
Figure 2. Myometrial I_{Na} model. Properties of I_{Na} are derived from experimental data of myometrial longitudinal cells [14,33,34,42] from late pregnant rats. A, V-dependent steady-states of activation (m_{∞}^3) and inactivation (h_{∞}); B, V-dependent time constants of activation (τ_m) and inactivation (τ_h). In both A and B, solid and empty circles are experimental data for activation and inactivation respectively. C, simulated I_{Na} at voltage steps of -40 to $0\,mV$ from a V_h of $-90\,mV$; D, simulated peak I–V relationship of I_{Na} at $V_h = -90\,mV$ and experimental I–V data. In both C and D, all data are normalized to the peak current value at $V = 0\,mV$.
doi:10.1371/journal.pone.0018685.g002

in human myometrial cells [13], which gives a maximal conductance $\bar{g}_{CaT}$ of $\approx 0.058 \, \mathrm{nS \, pF}^{-1}$. For incorporation of the I_{CaT} model in the later development of the USMC AP simulations, $E_{CaT} = 42 \, \mathrm{mV}$ so as to mimic that of Blanks *et al.*, [13].

Hyperpolarization-activated current – I_h

Mathematical description of the biophysical characteristics of this current are given in Appendix S1 (equations 35–39).

I_h has been reported in myometrial cells of pregnant rats [48,49]. Activated by hyperpolarization beyond resting membrane potential, I_h first appears at $V \approx -70 \, \mathrm{mV}$ from a V_h of $-50 \, \mathrm{mV}$. In the voltage-clamp experiments, activation of I_h is slow, taking $\geq 1 \, \mathrm{s}$, and it does not inactivate. It is more permeable to K^+ ions than Na^+ ions, is blocked by Cs^+, and has a reversal potential (E_h) of $\approx -20 \, \mathrm{mV}$.

I_h was modeled at room temperature to $30°C$ using myometrial cells of pregnant rats [48,49]. Our model of I_h biophysical characteristics was first developed with the data of [49] with an activation gating variable (y) and E_h approximated by the Goldman-Hodgkin-Katz (GHK) equation with a permeability ratio $P_{Na}/P_K = 0.35$. The half-activation was adjusted and the activation time constant was corrected with the reported $Q_{10} = 3.5$ [49] in order to match the experimental I–V relationship of Satoh [48] (Figure 4). The current density was $1.03 \, \mathrm{pA \, pF}^{-1}$ at $V = -120 \, \mathrm{mV}$ from a V_h of $-50 \, \mathrm{mV}$ [48], which gives a maximum conductance of $\bar{g}_h = 0.0542 \, \mathrm{nS \, pF}^{-1}$.

Potassium Currents

We have considered the electrophysiological data of several major types of potassium currents described from myometrial cells of rat and human myometrium: (two) voltage-gated potassium currents (I_{K1} and I_{K2}), A-type transient potassium current (I_{Ka}) and Ca^{2+}-activated potassium currents ($I_{K(Ca)}$). The kinetics of individual potassium currents are described in detail below; their current densities are discussed in the later section concerned with total potassium current.

Voltage-dependent potassium currents – I_{K1} and I_{K2}

Mathematical descriptions of the biophysical characteristics of these currents are given in Appendix S1 (equations 40–58).

Myometrial potassium currents have been roughly categorized by their inactivation properties and sensitivity to pharmacological blockers of varying channel subtype specificity [17,19]. At least two different types of potassium currents with rectifying properties were found in myometrial cells of late pregnant rats [17] and humans [19]; their dynamics were very slow compared to other membrane currents in myometrial cells. These potassium currents were separated as *C1* and *C2* components of the total potassium current in Wang *et al.*, [17] and as I_{K1} and I_{K2} in Knock *et al.*, [19].

C1 and I_{K1}, and *C2* and I_{K2} have similar voltage-dependent kinetics. Both *C1* and I_{K1} first appear at $V \approx -50$ to $-40 \, \mathrm{mV}$ and with half-inactivation ($V_{0.5,inact}$) between $-62 \, \mathrm{mV}$ to $-68 \, \mathrm{mV}$. Both *C2* and I_{K2} first appear at $V \approx -40$ to $-30 \, \mathrm{mV}$ and with $V_{0.5,inact}$ between $-30 \, \mathrm{mV}$ to $-20 \, \mathrm{mV}$. Wang *et al.*, [17] distinguished between *C1* and *C2* by their activation thresholds and inactivation properties whereas Knock *et al.*, [19] separated I_{K1} and I_{K2} by these properties *and* current sensitivities to 4-aminopyridine (4-AP) and TEA. As such, we developed mathe-
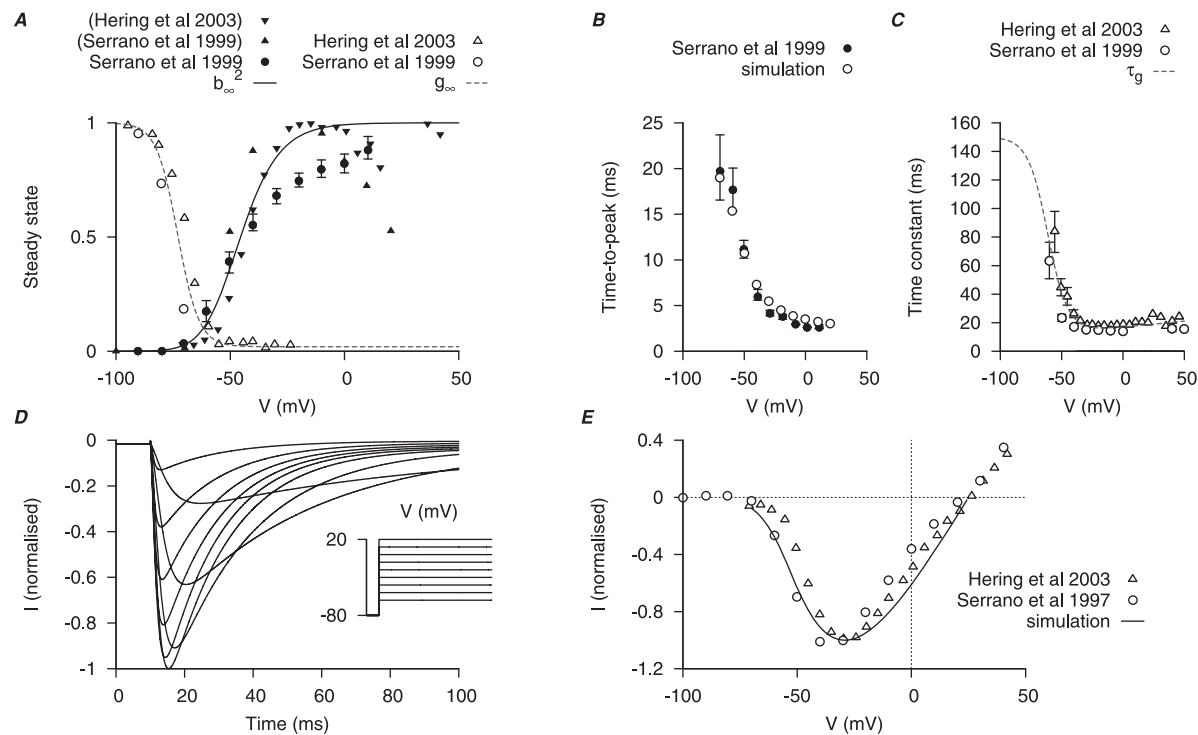
Figure 3. Myometrial I_{CaT} model. Properties of I_{CaT} are derived primarily from experimental data of Serrano *et al.*, [43] and Hering *et al.*, [44]. *A*, V-dependent steady-states of activation (b_∞^2) and inactivation (g_∞); experimental data in brackets were extrapolated from the published I–V relationships and normalized to the maximum value. *B*, superimposed simulated and experimental time-to-peak of I_{CaT} at different V stepped from V_h of $-100 \, \mathrm{mV}$; a function for the V-dependent activation time constant is chosen so that the simulated time-to-peak (*empty circles*) matched the experimental data (*solid circle*). *C*, V-dependent inactivation time constant (τ_g). *D*, simulated I_{CaT} at voltage steps of -60 to $20 \, \mathrm{mV}$ from a V_h of $-80 \, \mathrm{mV}$; *E*, simulated peak I–V relationship of I_{CaT} and experimental I–V data. In both *D* and *E*, all data are normalized to the peak current value at $V \approx -25 \, \mathrm{mV}$.
doi:10.1371/journal.pone.0018685.g003
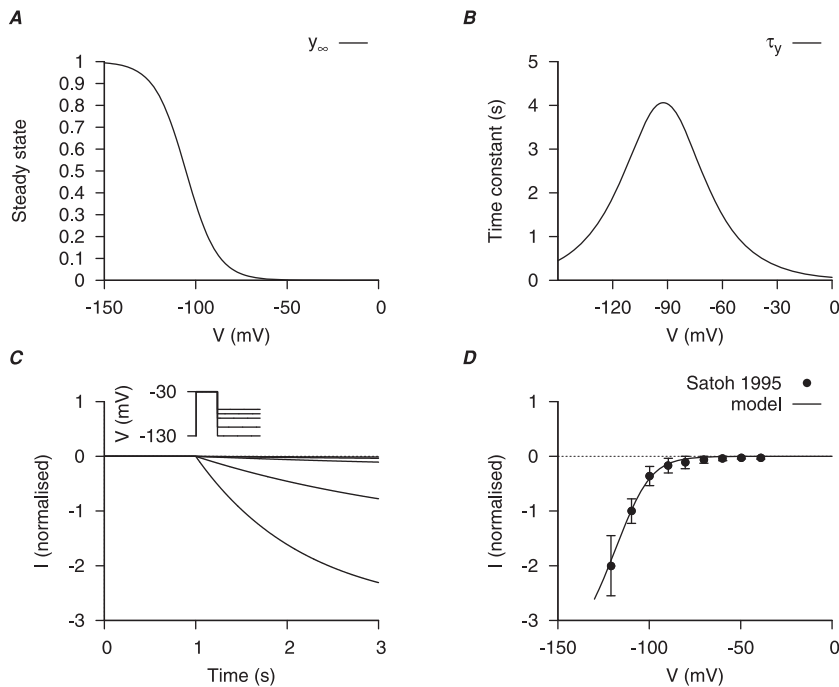
Figure 4. Myometrial I_h model. Properties of I_h are derived from experimental data of Okabe et al., [49] in rat circular myometrial cells and adjusted to experimental data of longitudinal cells [48]. *A*, V-dependent activation steady-state (y_∞); *B*, V-dependent activation time constant (τ_y). *C*, simulated voltage-clamp I_h at voltage steps of -130 to $-70\,mV$ from a holding potential of $-30\,mV$. *D*, simulated I–V relationship of I_h and experimental I–V data Satoh [48]. In both *C* and *D*, all data are normalized to the current value at V = 110 mV.
doi:10.1371/journal.pone.0018685.g004

matical models predominantly based upon the more abundant information of electrophysiological characteristics of human myometrial I_{K1} and I_{K2} and complemented these with data on rat myometrial *C1* and *C2* of Wang *et al.*, [17] at room temperature.

The equations of I_{K1} (not to be confused with the myocardial inward rectifying potassium current commonly designated also as I_{K1} [50]) and I_{K2} each incorporate three gating variables: an activation gating variable (q for I_{K1}; p for I_{K2}), a fast inactivation gating variable (r_1 for I_{K1}; k_1 for I_{K2}) and a slow inactivation gating variable (r_2 for I_{K1}; k_2 for I_{K2}). The activation and inactivation steady-state values were used as reported from Wang *et al.*, [17] with the assumption that both currents were completely inactivated (Figure 5A, 6A, see below). For I_{K1}, voltage-dependent steady-state of inactivation (r_∞) is formulated with the reported half-inactivation of $-63\,mV$ and slope factor of $6.3\,mV$ and, for I_{K2}, voltage-dependent steady-state of inactivation (k_∞) is assessed with the reported half-inactivation of $-21.2\,mV$) and slope factor of $5.7\,mV$ reported by Wang *et al.*, [17].

Activation time constants of I_{K1} and I_{K2} currents were from Knock *et al.*, [19] (Figure 5B, 6B) for I_{K1} and I_{K2} respectively. However, Knock *et al.*, [19] reported the inactivation time constants of I_{K1} and I_{K2} currents elicited at only one voltage step (V_h of $-80\,mV$ stepped to $+10\,mV$): inactivation of I_{K1} was described as a double exponential and a constant whereas inactivation of I_{K2} was described as a monoexponential and a constant. Their inclusion of constant values was due to the currents not inactivating during the course of the 10 sec voltage pulse. However, using these values it was impossible to simulate the published raw current tracings of the voltage-clamp protocols for I_{K1} and I_{K2} (Figure 4 in Knock *et al.*, [19]). We therefore sought to extract a more complete set of inactivation time constants that encompassed currents elicited at each voltage step

of the protocols listed in Knock *et al.*, [19]. This was accomplished by examining the raw data tracings kindly supplied by Drs Greg Knock and Phil Aaronson (Kings College London). The I_{K1} or I_{K2} currents in each of these datasets were produced in $10\,mV$ steps between $-50\,mV$ and $10\,mV$ from a V_h of $-80\,mV$. Averaging the I_{K1} (5 cells, Figure S4) or I_{K2} (4 cells, Figure S5) at each step enabled a calculation of the voltage-dependent inactivation time constants (Figure 5C and 6C for I_{K1} and I_{K2} respectively). The inactivations of I_{K1} and I_{K2} were described by a fast and a slow time constants. Moreover, we removed the need for a constant value used by Knock *et al.*, [19] by assuming that each current was completely inactivated. This, in fact, was reported to be the case by Knock *et al.*, [19] when they extended the experimental voltage pulses beyond 10 seconds. Satisfactory simulation of the published I–V curves and raw current data was now possible. Simulated I–V relationships of I_{K1} and I_{K2} (Figure 5D, 6D) stepping from two different V_h, $-80\,mV$ and $-40\,mV$, showed that while I_{K1} was mostly inactivated with $V_h = -40\,mV$, I_{K2} remained available. From the simulated current tracings (Figure 5E, 6E) both I_{K1} and I_{K2} took more than $10\,s$ to inactivate but I_{K2} was inactivated faster than I_{K1}. Current densities of I_{K1} and I_{K2} are discussed in the section of total potassium current.

A-type transient potassium current – I_{Ka}

Mathematical descriptions of the biophysical characteristics of this current are given in Appendix S1 (equations 59–65).

I_{Ka} is a 4-AP sensitive, TEA-insensitive potassium current with very fast activation and inactivation kinetics. It is found in myometrial cells of both rat and human [27,51].

I_{Ka} is first evident at V $\approx -40\,mV$ and raw data tracings show I_{Ka} peak activation within $\approx 10\,ms$ and almost completely inactivated within $50\,ms$ [27,51]. In human myometrial cells, I_{Ka} has a half-inactivation of $\approx -70\,mV$ and a slope factor of
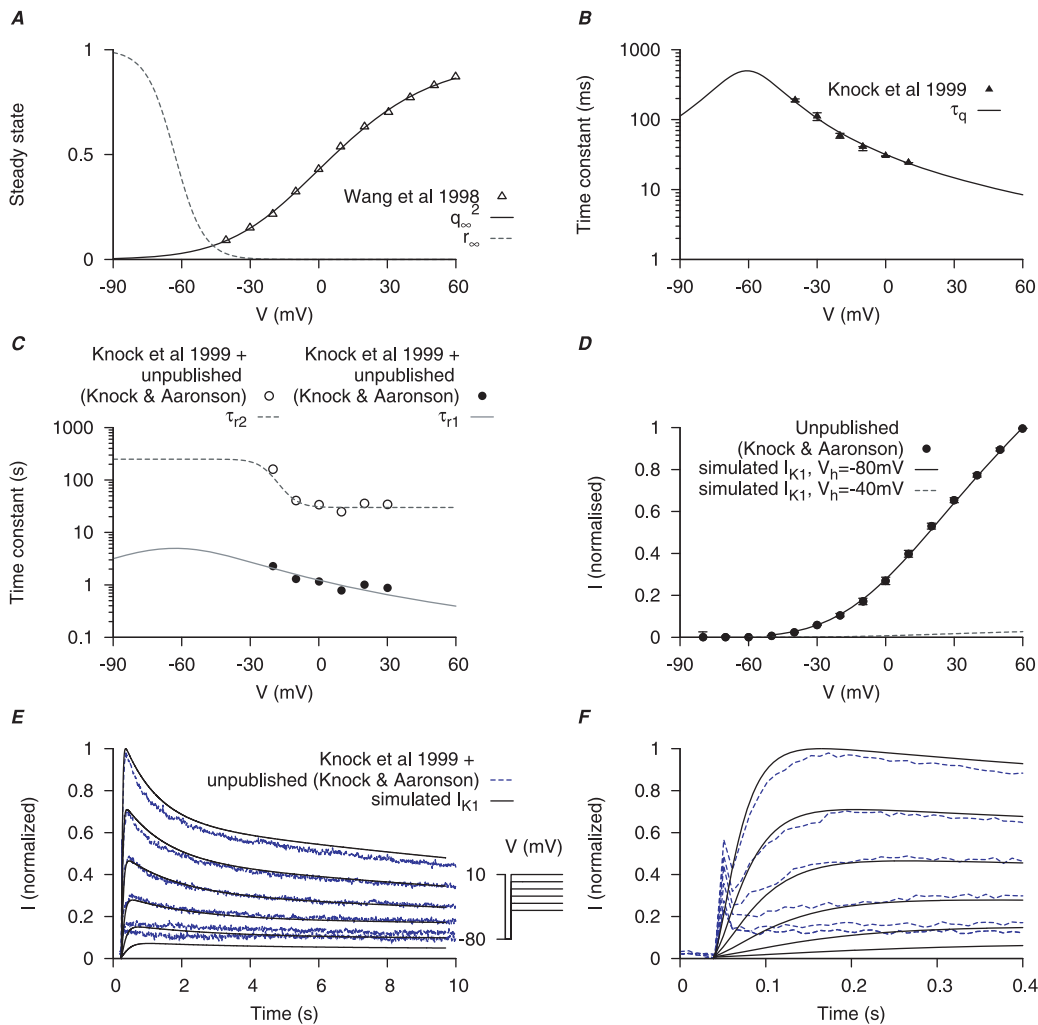
Figure 5. Myometrial I_{K1} model. Steady-state properties of I_{K1} are derived from experimental data of myometrial longitudinal cells in late pregnant rats [17]; the kinetics are from myometrial cells in late pregnant women from Knock et al., [19] and Knock G & Aaronson P (personal communication, including unpublished time tracings - see Figure S4). A, V-dependent steady-states of activation ($q_\infty{}^2$) and inactivation (r_∞). B, V-dependent activation time constants (τ_q). C, V-dependent fast (τ_{r1}) and slow (τ_{r2}) inactivation time constants. The experimental fast (*solid circles*) and slow (*empty circles*) inactivation time constants were extracted by fitting voltage-clamp time tracings averaged from five cells (1 published and 4 unpublished with the average values labeled as 'Knock et al 1999+unpublished (Knock & Aaronson)' in the figure). D, simulated I–V relationship of I_{K1} from holding potentials of $-80\,\mathrm{mV}$ and $-40\,\mathrm{mV}$ with $[K^+]_o = 5\,\mathrm{mM}$ and $[K^+]_i = 110\,\mathrm{mM}$; all values are normalized to the peak current at $V = 60\,\mathrm{mV}$ from $V_h = -80\,\mathrm{mV}$. E, simulated time tracings and averaged raw data of I_{K1} at voltage steps of -40 to $10\,\mathrm{mV}$ from V_h of $-80\,\mathrm{mV}$; both simulated and experimental currents are normalized to the peak current at $10\,\mathrm{mV}$; F, enlarged E showing activation of I_{K1} during the first few hundred milli-seconds.
doi:10.1371/journal.pone.0018685.g005

$\approx 5\,\mathrm{mV}$ [19,51]. These characteristics are very similar to the transient potassium current in myometrial cells isolated from immature rats [52] which were inhibited by $1\,\mathrm{mM}$ of 4-AP and were measured within $3-6\,\mathrm{ms}$ of the voltage step; it has a half-inactivation of $\approx -48\,\mathrm{mV}$ and a slope factor of $8.7\,\mathrm{mV}$.
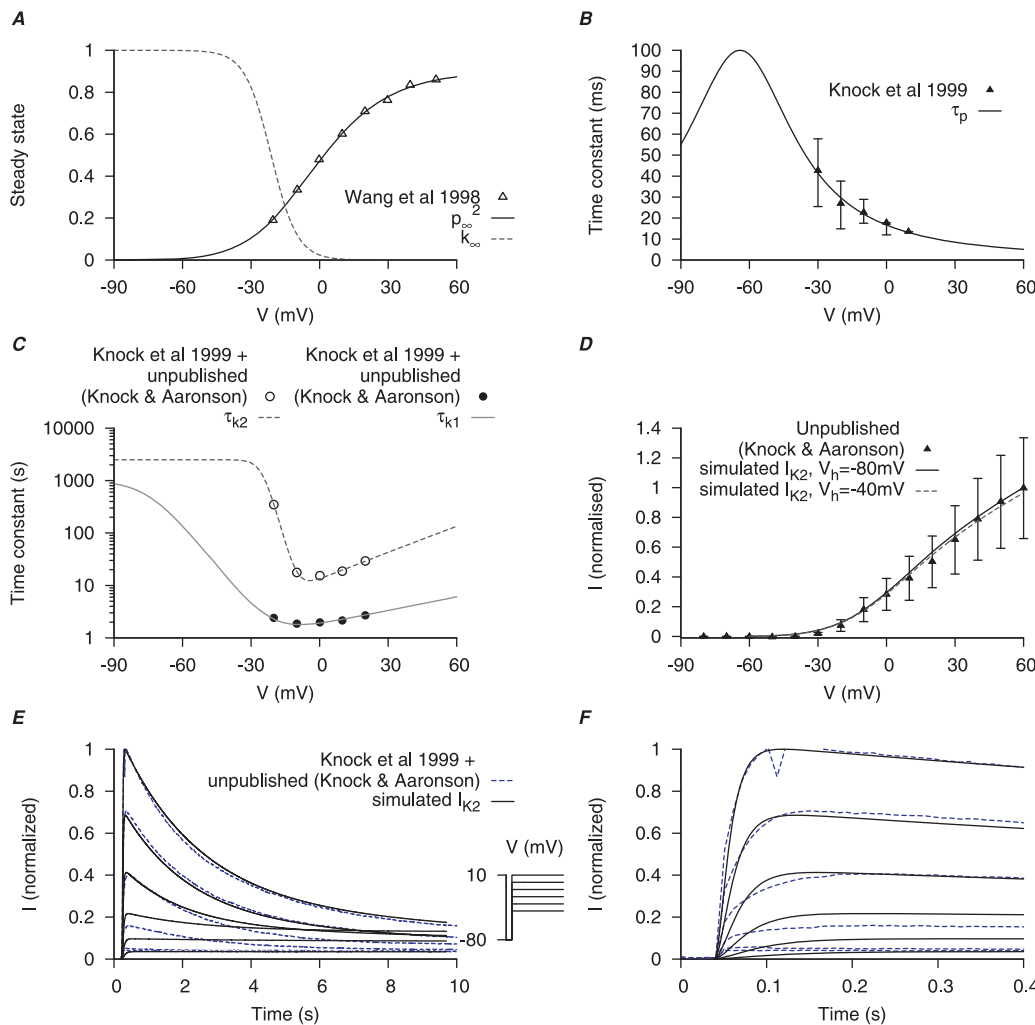
I_{Ka} is modeled from data of myometrial cells from pregnant rats and humans recorded at room temperature. The model of I_{Ka} incorporates one activation gating variable (s) and an inactivation gating variable (x). Steady-state values for activation and inactivation are shown in Figure 7A. Voltage-dependent steady-state of inactivation x_∞ is formulated with the reported half-inactivation of $-69.5\,\mathrm{mV}$ and slope factor of $6\,\mathrm{mV}$ reported by Knock et al., [19]. The activation time constants were chosen to fit the time-to-peak experimental data (Figure 7B). Experimental values of steady-state and time-to-peak are kindly provided by Drs

Greg Knock and Phil Aaronson (Kings College London). The inactivation time constants were obtained by fitting the raw data current tracings from Knock et al., [51] and the simulated time tracings showed dynamics similar to the experimental time tracings (Figure 7C). The simulated I–V relationship shows that I_{Ka} first appears at $V \approx -40\,\mathrm{mV}$, similar to experimental data [51] (Figure 7D). Current density of I_{Ka} is discussed in the section of total potassium current.

Calcium-activation potassium current – $I_{K(Ca)}$

Mathematical descriptions of the biophysical characteristics of this current are given in Appendix S1 (equations 66–78).

Calcium-activated potassium currents ($I_{K(Ca)}$) have been suggested to play important roles in suppressing the excitability of smooth muscle cells especially those in the vasculature. In

Figure 6. Myometrial I_{K2} model. Steady-state properties of I_{K2} are derived from experimental data of myometrial longitudinal cells in late pregnant rats [17]; the kinetics are extracted from raw data tracings from myometrial cells of late pregnant women from Knock *et al.*, [19] and Knock G & Aaronson P (personal communication, including unpublished time tracings - see Figure S5). *A*, V-dependent steady-states of activation (p_∞^2) and inactivation (k_∞). *B*, V-dependent activation time constants (τ_p) *C*, V-dependent fast (τ_{k1}) and slow (τ_{k2}) inactivation time constants. The experimental fast (*solid circles*) and slow (*empty circles*) inactivation time constants were extracted from voltage-clamp time tracings averaged from four cells (1 published and 3 unpublished with the average values labeled as 'Knock et al 1999+unpublished (Knock & Aaronson)' in the figure. *D*, simulated I–V relationship of I_{K2} from a holding potential of -80 mV and -40 mV with $[K^+]_o = 5$ mM and $[K^+]_i = 110$ mM; all values are normalized to the peak current at V = 60 mV from $V_h = -80$ mV. *E*, simulated time tracings of I_{K2} at voltage steps of -40 to 10 mV from a holding potential of -80 mV; both simulated and experimental currents are normalized to the peak current at 10 mV; *F*, enlarged *E* showing activation of I_{K2} during the first few hundred milli-seconds.

doi:10.1371/journal.pone.0018685.g006

myometrial cells $I_{K(Ca)}$ is under complex gestational-mediated regulation: the large conductance Ca^{2+}-activated K^+ channels (termed BK_{Ca} channel) subunit compositions and current density are diminished near to term. As such, although BK_{Ca} channels have been a focus of much interest in the myometrium [16,17,19,53–62], detailed biophysical information on $I_{K(Ca)}$ whole cell current is rather restricted.

When detected in myometrial whole cell recordings, $I_{K(Ca)}$ was distinctly noisy and its activation was almost instantaneous [17,27]. From the reported recordings of $I_{K(Ca)}$ in myometrial cells by Khan *et al.*, [16,61,62], Wang *et al.*, [17] and Noble *et al.*, [20] many of the biophysical parameters required to model complete ion current characteristics are absent. Therefore, a biophysical quantification of the $I_{K(Ca)}$ current is developed from experimental whole cell electrophysiological data obtained at room temperature

from cloned mammalian smooth muscle α (pore-forming) and $\beta1$ (regulatory) subunits of BK_{Ca} subsequently expressed in *Xenopus laevis* oocytes [63,64]. The current densities of $I_{K(Ca)}$ in the model are adjusted to replicate published human myometrial cell data [65,66].

We assumed that the transmembrane $\beta1$ subunits were separately regulated from the pore-forming α subunits and, therefore, two subtypes of $I_{K(Ca)}$ were developed: one where I_α reflects an $I_{K(Ca)}$ consisting of α subunits; another where $I_{\alpha\beta1}$ represents an $I_{K(Ca)}$ consisting of α and $\beta1$ subunits; the total $I_{K(Ca)}$ is then taken as the sum of I_α and $I_{\alpha\beta1}$. This also enabled investigation of the effects of changing voltage- and calcium-sensitivities of $I_{K(Ca)}$.

The conductances of I_α and $I_{\alpha\beta1}$ are each modeled by an activation gating variable (x_α for I_α; $x_{\alpha\beta1}$ for $I_{\alpha\beta1}$). The half-
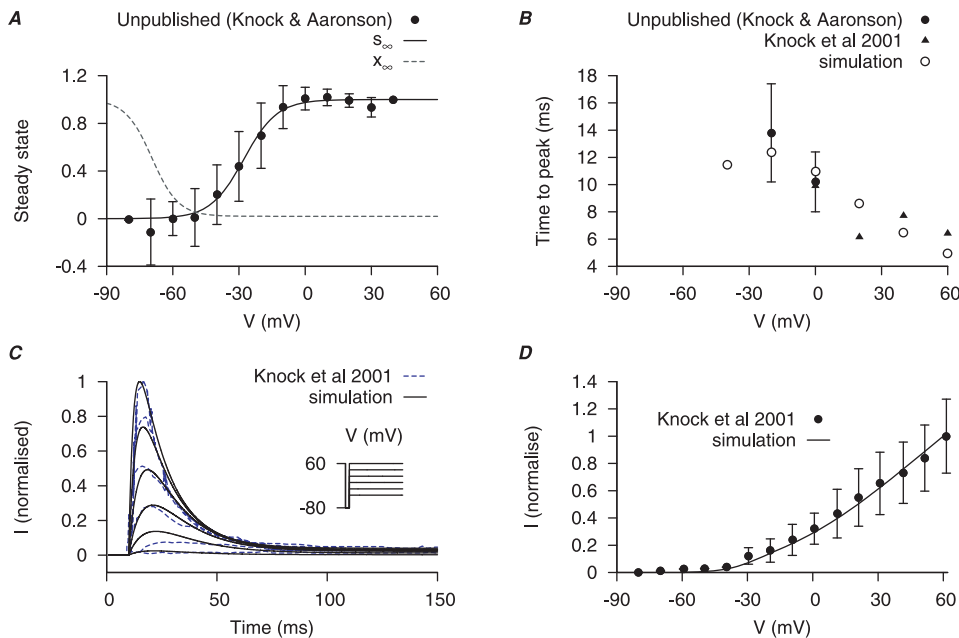
Figure 7. Myometrial I_{Ka} model. Properties of I_{Ka} are derived from experimental data of myometrial cells from Knock *et al.*, [19,51] and Knock G & Aaronson P (unpublished data, personal communication) in late pregnant women. Functions for V-dependent activation and inactivation time constants are chosen so that the simulated time-to-peak, current tracings and I–V relationship matched the experimental data. *A*, V-dependent steady-states of activation (s_∞) and inactivation (x_∞). *B*, simulated (*empty points*) and experimental (*solid points*) time-to-peak of I_{Ka} at different V stepped from a V_h of -80 mV. *C*, simulated voltage-clamp I_{Ka} at voltage steps of -40 to 60 mV from a holding potential of -80 mV are superimposed on experimental current tracings from Knock *et al.*, [51]; *F*, simulated peak I–V relationship of I_{Ka} and experimental I–V data. In both *E* and *F*, all data are normalized to the peak current value at V $= 60$ mV.
doi:10.1371/journal.pone.0018685.g007

activation and the corresponding gating charge were functions of $[Ca^{2+}]_i$ (Figure 8A); the simulated activation steady-states in comparison to the experimental values at different $[Ca^{2+}]_i$ [63,64] are shown in Figure 8B and the activation time constants in Figure 8C. A ratio of 70% I_α to 30% $I_{\alpha\beta1}$ was found to produce the best fit of myometrial cell experimental I–V relationships [65,66]. Using estimates of resting and peak global $[Ca^{2+}]_i$ in myometrial cells of 100 nM and 800 nM respectively [67], the simulated I–V curves showed that high $[Ca^{2+}]_i$ increased $I_{K(Ca)}$ at positive membrane potentials (Figure 8D). Current density of $I_{K(Ca)}$ is discussed in the section of total potassium current.

Background potassium current – I_b

Mathematical description of the biophysical characteristics of this current are given in Appendix S1 (equation 79).

We have described so far the biophysical properties of the major myometrial K^+ currents for which there is sufficient detailed electrophysiological information (I_{K1}, I_{K2}, I_{Ka} and $I_{K(Ca)}$). Other, less biophysically detailed electrophysiological information, together with evolving molecular and pharmacological data, suggests the possible existence of other myometrial K^+ current sub-types including small-conductance Ca^{2+}-activated K^+ channels (termed $SK_{(Ca)}$) and voltage-dependent Kv7 (KCNQ) channels [20,68–71]. Therefore, I_b, a linear background potassium current is added and it collectively represents the remaining K^+ currents.

Whole cell total potassium current – I_K

In order to model the whole cell I_K it is necessary to combine the current densities of each of the potassium current components.

The current densities of voltage-gated potassium currents (I_{K1} and I_{K2}) reported in myometrial cells show considerable variability. The total voltage-gated potassium current at the voltage step of 60 mV, from V_h between -80 mV and -100 mV in myometrial cells studied by Knock *et al.*, [19,51] varied between $\approx 8-12$ pA pF^{-1}. Interestingly, the majority of human myometrial cells consisted of either I_{K1} (24/42 cells) or I_{K2} (18/42 cells) as the dominant potassium current [19] with only a very small number of myometrial cells reported to exhibit both I_{K1} and I_{K2} [51]. In contrast, Wang *et al.*, [17] reported a voltage-gated potassium current density of 40.1 pA pF^{-1} at 70 mV from V_h of -80 mV. The potassium current was a mixture of 67% *C1* (corresponding to I_{K1} in Knock *et al.*, [19]) and 23% *C2* (corresponding to I_{K2} in Knock *et al.*, [19]) and, together, they accounted for almost 90% of total potassium current during a 10 s voltage step; the remaining 10% were sustained currents consisting of mostly $I_{K(Ca)}$ with an activation threshold of V > 0 mV.

The reported peak current for I_{Ka} ranges between $\approx 2-4$ pA pF^{-1} in human myometrial cells [51] and ≈ 18 pA pF^{-1} in rat myometrial cells [27] at voltage steps of $40-60$ mV from a V_h of -80 mV. However, from the raw time tracing [27,51], the ratio of the peak I_{Ka} (occurring at ≈ 10 ms) with respect to the peak total potassium current (occurring at ≈ 50 ms) was consistent at $\approx 0.34-0.44$ over a range of voltage steps from -10 mV to $+40$ mV. Therefore, the maximal conductance of I_{Ka} was chosen so that the peak of I_{Ka} corresponds to 40% of the peak total potassium current (Figure 9A).

We have chosen the maximal conductances of I_{K1}, I_{K2}, I_{Ka}, $I_{K(Ca)}$ and I_b such that, together, the simulated total potassium current under different voltage-clamp protocols fits the profiles of experimental voltage-clamp results in Miyoshi *et al.*, [27] and Wang *et al.*, [17] (Figure 9).

In the later development of the USMC AP simulations, the total potassium current density was scaled to match the experimental
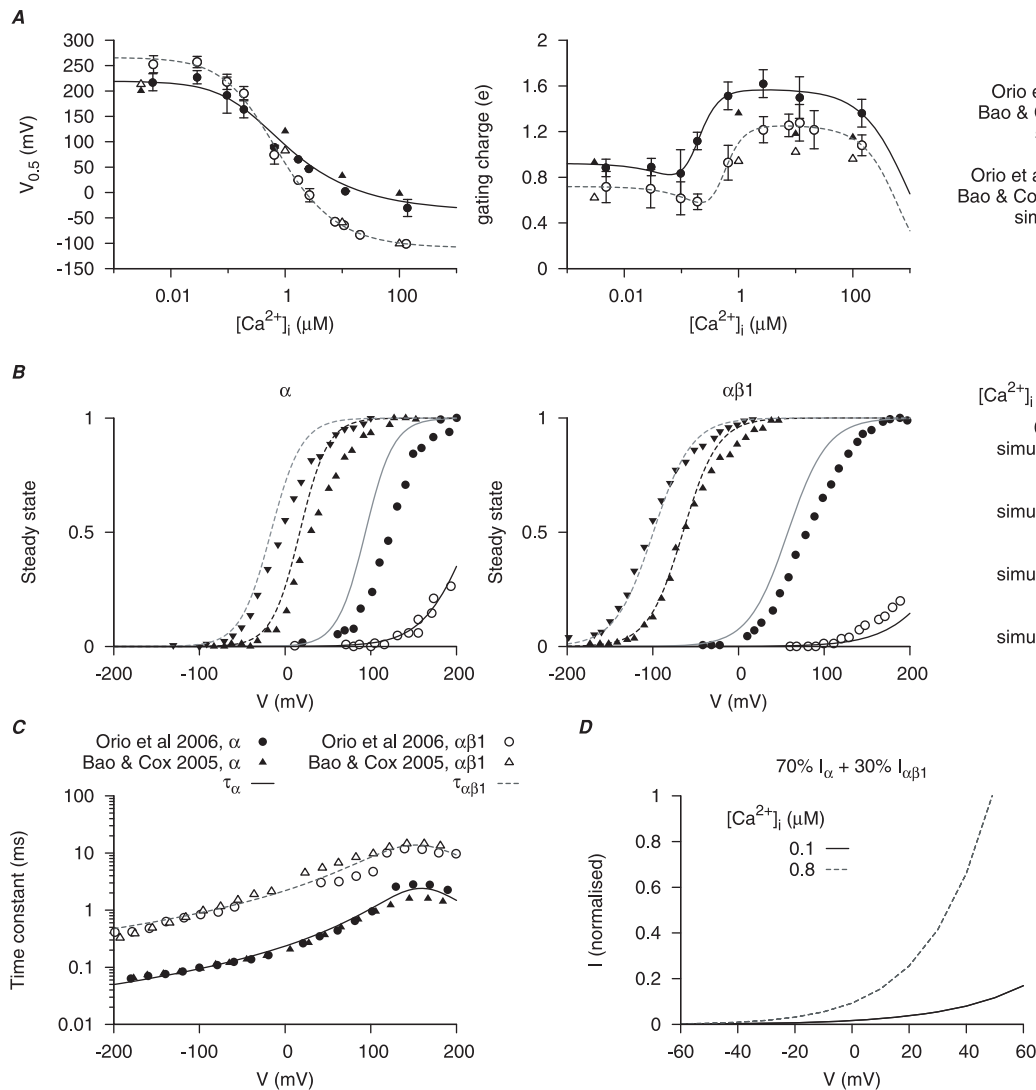
Figure 8. Myometrial $I_{K(Ca)}$ model. The calcium- ($[Ca^{2+}]_i$), voltage- (V) and time-dependent kinetics for the two types of $I_{K(Ca)}$ currents, I_α and $I_{\alpha\beta1}$, are developed with experimental data from cloned mammalian myometrial and smooth muscle MaxiK α and $\beta1$ subunits expressed in *Xenopus laevis* oocytes [63,64]; the current density and proportion of $I_\alpha : I_{\alpha\beta1}$ are adjusted with I–V relationships from different mammalian myometrial cells [17,65,66]. In A and C, solid and empty circles are experimental data for I_α and $I_{\alpha\beta1}$ respectively. A, $[Ca^{2+}]_i$-dependent half-activation ($V_{0.5}$) and activation gating charge. B, simulated activation steady-states for I_α and $I_{\alpha\beta1}$ at different $[Ca^{2+}]_i$; solid and empty circles are experimental data from Orio et al., [64] and Bao & Cox [63] respectively. C, V-dependent activation time constants for I_α and $I_{\alpha\beta1}$. D, simulated I–V relationships of $I_{K(Ca)}$ at anticipated myometrial resting and peak $[Ca^{2+}]_i$ levels, with the proportion of $I_\alpha : I_{\alpha\beta1} = 0.7 : 0.3$. Both I–V relationships are normalized to $I_{K(Ca)}$ at V = 60 mV at peak $[Ca^{2+}]_i$ level.
doi:10.1371/journal.pone.0018685.g008

data of whole cell potassium current in Okabe *et al.*, [32]; $\approx 4\,\mathrm{pA\,pF^{-1}}$ at V = 0 mV from a V_h of −50 mV.

Other membrane currents

A non-selective cation current (I_{NSCC}) and a calcium-activated chloride current ($I_{Cl(Ca)}$) have been reported for myometrial cells from late pregnant rats. We also formulated electrogenic currents for the Na^+-K^+ ATPase and Na^+-Ca^{2+} exchangers, I_{NaK} and I_{NaCa} respectively, by extrapolating data from other cell systems. I_{NaCa} will be discussed with $[Ca^{2+}]_i$ dynamics in a later section.

Calcium-activated chloride current – $I_{Cl(Ca)}$

Mathematical descriptions of the biophysical characteristics of this current are given in Appendix S1 (equations 80–86).

The presence of channels permeable to chloride in myometrial cells was first reported by Coleman & Parkington [72]. Subsequently, there have been several reports of calcium-activated chloride current in myometrial cells, albeit the biophysical characteristics have not been as thoroughly explored as in other smooth muscles and tissues [15,17,73,74]. In addition, Clca isoforms 3 and 4, suggested to encode for channel proteins responsible for $I_{Cl(Ca)}$, have been found in the uterus and the induced expression of Clca4 in mammalian cells elicited a calcium-dependent chloride current [75,76].

The only serious single cell electrophysiological assessment of $I_{Cl(Ca)}$ in myometrial cells (rat, 35°C) is from Jones *et al.*, [15] and therefore, this is the experimental data used for our modeling purposes. They used two different voltage-clamp protocols: a single step voltage-clamp and a two-step voltage-clamp (illustrated
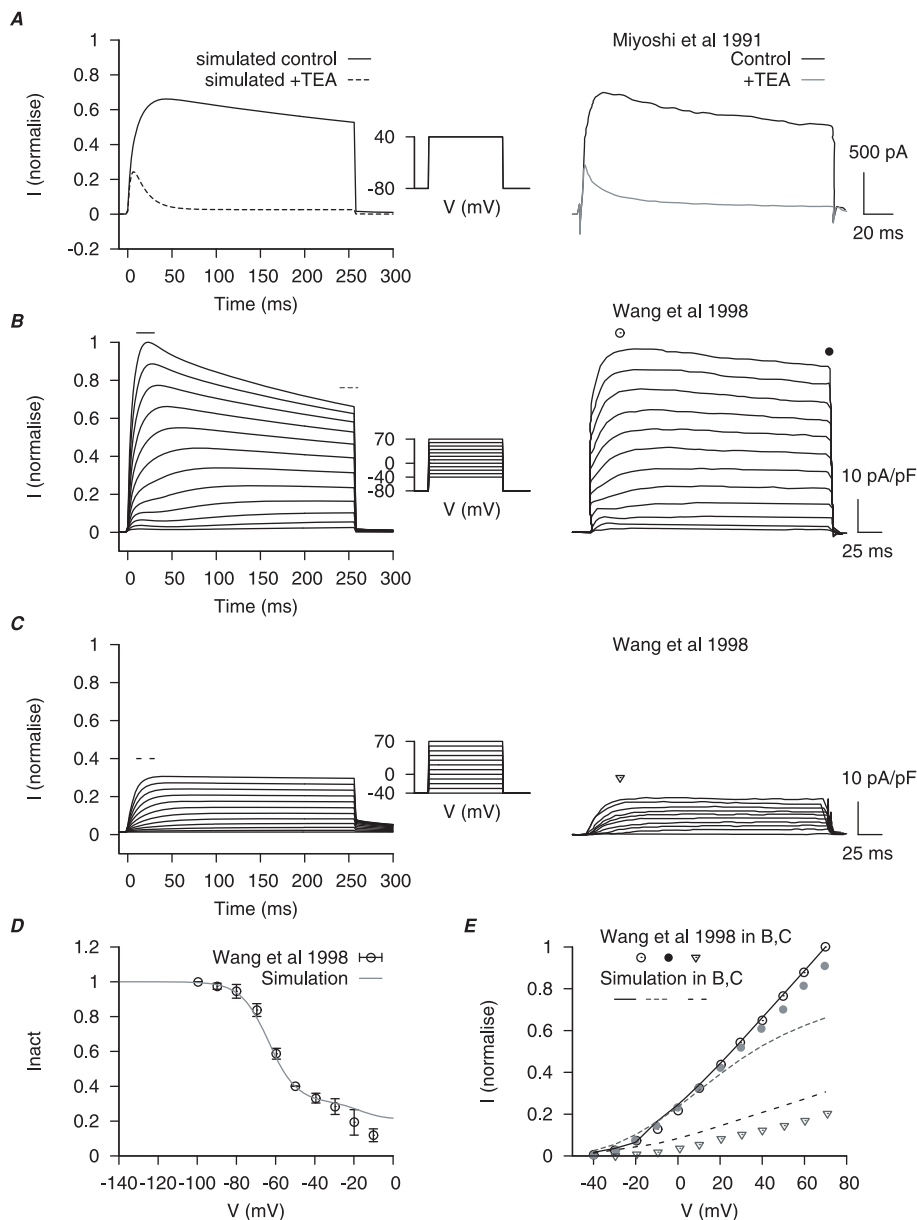
Figure 9. Myometrial total I_K model. Potassium currents including I_{K1}, I_{K2}, I_{Ka}, $I_{K(Ca)}$ and I_b were combined to simulate the whole cell I_K data of Miyoshi et al., [27] and Wang et al., [17]. A, simulated effects of 10 mM TEA (*left*), which blocks I_{K1}, I_{K2} and $I_{K(Ca)}$ but not I_{Ka}, at a voltage step of 40 mV from a holding potential (V_h) of -80 mV; corresponding experimental results [27] (*right*). B, simulated whole cell potassium currents (*left*) and corresponding experimental results [17] (*right*) at voltage steps from -40 mV to 70 mV from a V_h of -80 mV; and C, from a V_h of -40 mV. D, simulated inactivation of whole cell potassium currents with the same two-step protocol in Wang et al., [17]: $V_h = -80$ mV, followed with a 10 s conditional step ranging from -140 mV to 0 mV, then a final test step at 70 mV for 180 ms. The peak current during the the test steps is normalized to test step at -140 mV. E, the I–V relationships at peak and at the end of the voltage step in B and C. In B and C, simulated currents are normalized to the peak current at V = 70 mV from $V_h = -80$ mV.
doi:10.1371/journal.pone.0018685.g009

in Figures 1 and 2, respectively, of Jones *et al.*, [15]). Both protocols relied on the activation of I_{CaL} to raise $[Ca^{2+}]_i$ which, in turn, was proposed to activate $I_{Cl(Ca)}$. $[Ca^{2+}]_i$, however, was not clamped in Jones *et al.*, [15] and so, for modeling purposes, it was not possible to determine the steady-state values nor the activation kinetics. However, such information is available from the data of Arreola *et al.*, [77] for $I_{Cl(Ca)}$ in rat parotid acinar cells whereupon Ca^{2+} buffers were introduced intracellularly to control $[Ca^{2+}]_i$. This enabled the recording and modeling of calcium- and voltage-dependencies of $I_{Cl(Ca)}$. In addition, the Arreola *et al.*, [77] model

could reproduce the calcium- and voltage-dependencies of $I_{Cl(Ca)}$ in pulmonary vascular smooth muscle cells [78]. As such, we applied the model of Arreola *et al.*, [77] to simulate the myometrial data of Jones *et al.*, [15]. Utilizing the values for the calcium-dependent time constant of activation from Arreola *et al.*, [77], or even changing them substantially, failed to provide a suitable fit to the Jones *et al.*, [15] $I_{Cl(Ca)}$ dynamics. If one assumed only a voltage-dependency to the activation time constant then the raw data time tracings of Jones *et al.*, [15] could be fitted by the Arreola *et al.*, [77] model (Figure 10). Thus we include $I_{Cl(Ca)}$ in our later

model of USMC AP form with the caveat that the activation kinetics are different from that described in other cells [77,78].

## Non-selective cation current – I_{NSCC}

Mathematical descriptions of the biophysical characteristics of this current are given in Appendix S1 (equations 87–92).

Miyoshi *et al.*, [79] had identified a non-specific cation current in late pregnant rat myometrial cells. I_{NSCC} is a linear, time-independent cation current. It is permeable to K^+, Na^+, Cs^+ and Ca^{2+}, with relative permeability ratios of $P_K : P_{Cs} : P_{Na} : P_{Ca} = 1.3 : 1 : 0.9 : 0.89$. The conductance of I_{NSCC} depends on extracellular concentrations of permeable cations and it was inhibited by extracellular Mg^{2+}, La^{3+} and Gd^{3+}. The reported reversal potential and current density under standard conditions in

Miyoshi *et al.*, [79], with $0.1 \, mM \, [Mg^{2+}]_o$ and utilizing a voltage ramp protocol, were, respectively, $\approx -5 \, mV$ and $0.6 \pm 0.46 \, pA \, pF^{-1}$.

I_{NSCC} is modeled with data from late pregnant rat myometrial cells recorded at room temperature. The reversal potential of I_{NSCC} (E_{NSCC}) is approximated by the Goldman-Hodgkin-Katz (GHK) equation [80] with the reported permeability ratio [79]. Intracellular and extracellular concentrations of Cs^+ and NMDG with $P_{NMDG} : P_{Cs} = 0.2$ were included in the calculation of E_{NSCC} while fitting experimental data in Miyoshi *et al.*, [79]; these parameters for Cs^+ and NMDG were excluded in the later development of the USMC whole cell model.

The conductances of I_{NSCC} for different cations from the voltage ramp I–V relationships have a ratio of $Ca^{2+} : Na^+ :$
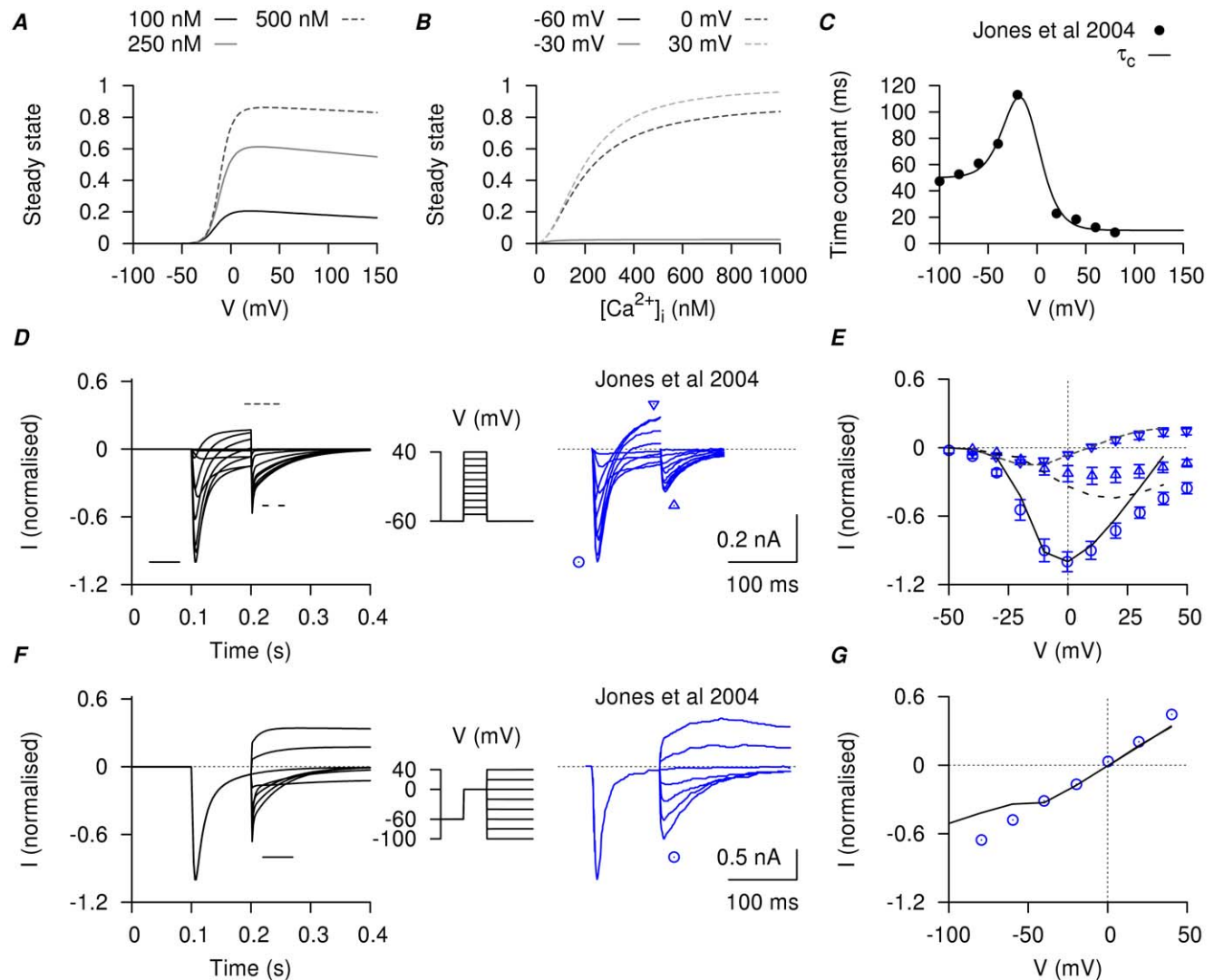
Figure 10. Myometrial $I_{Cl(Ca)}$ model. The steady-state of $I_{Cl(Ca)}$ is modified from Arreola *et al.*, [77]. *A*, steady-state of $I_{Cl(Ca)}$ with respect to V in three different $[Ca^{2+}]_i$ concentrations; *B*, steady-state of $I_{Cl(Ca)}$ with respect to $[Ca^{2+}]_i$ at four different membrane potentials. *C*, V-dependent activation time constant; the experimental data points are obtained by fitting the tail currents in figure 2 of Jones *et al.*, [15]. *D*, simulated currents (*left*) and the corresponding experimental currents in Jones *et al.*, [15] (*right*) elicited by a single-step voltage-clamp protocol (*inset*). The peak of the inward currents, the current values at the end of the voltage pulse, and the peak of the tail currents were marked for both simulated current (*lines*) and experimental current tracings (*circles*). *E*, I–V relationships, showing the marked peak at each voltage step in *D*. *F*, simulated currents (*left*) and the corresponding experimental currents in Jones *et al.*, [15] (*right*) by a two-step voltage-clamp protocol (*inset*). The peak of the tail currents were marked for both simulated current (*lines*) and experimental current tracings (*circles*). *G*, I–V relationships, showing the marked peaks of the tail currents at each voltage step in *F*. The simulated currents qualitatively reproduced the experimental current tracings in both voltage-clamp protocols, with almost zero net current at the holding potential and comparable amplitude and rate of decay of the tail currents.
doi:10.1371/journal.pone.0018685.g010

$K^+ : Cs^+ = 0.5 : 1 : 1.19 : 1.6$ [79]. Similar to I_{NSCC} in guinea-pig endocardial endothelial cells [81], conductance of myometrial I_{NSCC} was reduced with decreasing $[Na^+]_o$. With reference to Manabe et al., [81], this relationship was described by a Hill equation with a half-saturating concentration of 150 mM and a Hill coefficient of 2. We have normalized the Hill equation with the Na^+ conductance at 125 mM $[Na^+]_o$ and we assumed the same relationship held for other permeable cations; for Ca^{2+} ions, the Hill equation is normalized to the Ca^{2+} conductance observed at 20 mM $[Ca^{2+}]_o$. Inhibition by $[Mg^{2+}]_o$ is described by a Hill equation with a half-saturating concentration of 0.28 mM and a Hill coefficient of 1.3 [79]. I_{NSCC} is also permeable to other cations ions [79] and, therefore, a small leak component ($\bar{g}_L$) in its conductance is needed to match the experimental voltage ramp data. Under physiological conditions with 0.1 mM $[Mg^{2+}]_o$ the simulated I_{NSCC} consists of mostly Na^+ and leak components.

Sodium potassium pump current – I_{NaK}

Mathematical descriptions of the biophysical characteristics of this current are given in Appendix S1 (equations 93–96).

Evidence of Na^+-K^+ pump activity has been reported in myometrial cells of late pregnant rats [82–84] and human [8]. mRNA and protein expression corresponding to α and β subunits of the Na^+-K^+ ATPase have been reported in rodent and human myometrium with isoform-specific changes associated with advancing gestation and/or estrogen treatment [21,84–86]. In sodium-rich myometrial tissues of late pregnant rats [82,83] and human [8], changes of the membrane potential were sensitive to ouabain, the absence of external potassium or intracellular sodium and to low temperature, results that are suggestive of an electrogenic I_{NaK}. Despite this molecular and biophysical data supporting a role of the Na^+-K^+ pump in regulating myometrial activity, there is little information about the biophysical properties of I_{NaK} current in myometrial cells. Therefore, we adopted the formulation of an electrogenic I_{NaK} from rodent myocardial cells [87], which was dependent on membrane voltage, $[K^+]_o$, $[Na^+]_i$ and $[Na^+]_o$. The parameter values of voltage, $[K^+]_o$ and $[Na^+]_i$ dependencies, as well as current densities, are then fitted with the experimental data from rodent vascular smooth muscle cells [88] at 36°C. A Q_{10} value of 1.87 for 10°C change between $26-36$°C is reported for vascular smooth muscle cells [88]. We assumed the same $[Na^+]_o$ dependency with I_{NaK} in smooth muscle cells as in the myocardial cells.

Calcium fluxes

Mathematical descriptions of the plasmalemmal Ca^{2+} fluxes are given in the Methods (equation 7) and Appendix S1 (equations 97–103).

In myometrial cells from near-term pregnant rats, intracellular Ca^{2+} ions are removed from the cytoplasm principally by the plasmalemmal Ca^{2+}-ATPase (PMCA) and Na^+-Ca^{2+} exchanger [12,67,89,90]. From the decay rate constants, $\approx 60-70\%$ of cytoplasmic Ca^{2+} removal was estimated to be via the Na^+-Ca^{2+} exchanger and sequestration into intracellular stores, and 30% via PMCA when the cell was stimulated by ten short depolarization pulses between -80 mV and 0 mV [67].

We modified a myometrial intracellular calcium model [24] for inclusion in the development of the USMC AP simulations by incorporating time-dependent kinetics from membrane calcium currents. We also modified the formulation of the Na^+-Ca^{2+} exchanger to overcome its limits in fitting published Ca^{2+} decay tracings. For example, we found that the calcium decay tracings in Shmigol et al., [67] and Shmigol et al., [12] could only be fitted by the procedure described in Bursztyn et al., [24] with $[Na^+]_i = 16.55$ mM. However, no sodium ions were included in the pipette

(intracellular) solution used by Shmigol et al., [67]. The resultant reversal potential of the Na^+-Ca^{2+} exchanger was predicted at ≈ -90 mV which would mean the Na^+-Ca^{2+} exchanger **bringing in** extracellular calcium at resting membrane potentials of -50 mV to -80 mV which is incorrect. Our use of the well-described formula of Weber et al., [91] obviated this and enabled us to fit the Ca^{2+} fluxes with the same ionic concentrations used in Shmigol et al., [67] and Shmigol et al., [12]. With $[Na^+]_i = 0$ mM, the resultant reversal potential was in the positive membrane potential range and, thus, the Na^+-Ca^{2+} exchanger was predicted to **extrude** intracellular Ca^{2+} in the physiological range of resting membrane potentials.

We have modeled three major plasmalemmal calcium fluxes: the voltage-dependent membrane channels permeable to Ca^{2+} ($J_{Ca,mem}$); the Na^+-Ca^{2+} exchanger (J_{NaCa}); and the PMCA (J_{PMCA}).

The parameters for J_{NaCa} and J_{PMCA} are refitted with experimental results of calcium decay in late pregnant rat myometrial cells recorded at 35°C from Shmigol et al., [12,67]; the modified calcium sub-system is further validated with experimental data (Figure S7A). Details of individual fluxes are described below.

Membrane Ca^{2+} channels – $J_{Ca,mem}$

$J_{Ca,mem}$, which includes all the membrane ion channel calcium currents: I_{CaL}, I_{CaT} and the calcium component of I_{NSCC} ($I_{NSCC,Ca}$), was calculated from the total membrane calcium current as described in the Methods (equation 7).

Sodium-calcium exchanger – J_{NaCa}

The Na^+-Ca^{2+} exchanger has been suggested to be involved in calcium translocation in myometrial cells from pregnant rats [12,67,89,90]. However, it is unknown whether the myometrial Na^+-Ca^{2+} exchanger is electrogenic although the earliest studies of the effects of changing $[Na^+]_o$ and $[Ca^{2+}]_o$ on the rat myometrial cell membrane properties suggested so [92].

There are three Na^+-Ca^{2+} exchanger isoforms (NCX1, NCX2, NCX3) and NCX mRNA and protein has been reported in myometrium [93,94]. NCX2 is the predominantly expressed isoform in smooth muscle tissues, including the uterus, but its stoichiometry and electrogenicity are unknown. Cloning of NCX2 [95] shows that it shares $\approx 80\%$ similarity in amino acid sequences with NCX1, the predominant isoform in heart tissues, and they were functionally similar with respect to their I–V relationship and voltage-dependency [96,97]. Compared to NCX1, NCX2 has a higher dissociation rate (K_d) for Ca^{2+} at $K_{d,Cai} = 1.5$ μM and a lower $[Na^+]_i$ affinity at $K_{d,Nai} = 28$ μM. As the Na^+-Ca^{2+} exchangers in cardiac myocytes [98] and aortic smooth muscle cells are electrogenic [99] and the properties of NCX1 and NCX2 isoforms are similar, we presumed the myometrial sodium calcium exchanger would also be electrogenic.

We used an electrogenic Na^+-Ca^{2+} exchanger equation for cardiac cells from Weber et al., [91] that describes current dependencies on membrane potential, intra- and extra-cellular calcium and sodium concentrations and has a stoichiometry of $Na^+ : Ca^{2+} = 3 : 1$. Dissociation constants for $[Ca^{2+}]_i$ and $[Na^+]_i$ were set as $K_{d,Cai} = 1.5-7$ μM and $K_{d,Nai} = 28$ μM, respectively [22,95]. Dissociation constants for $[Ca^{2+}]_o$ and $[Na^+]_o$ were assumed the same as Weber et al., [91]. The maximum calcium flux via J_{NaCa} and parameters for $[Ca^{2+}]_i$ allosteric activation were refitted with experimental results of calcium decay in late pregnant rat myometrial cells [12,67]. Membrane current from the Na^+-Ca^{2+} exchanger, I_{NaCa}, is converted from the fitted calcium fluxes J_{NaCa}.

Plasma membrane Ca^{2+} ATPase – J_{PMCA}

PMCA activity in rat myometrial cells has been characterized in fractionated plasma membranous vesicles with a reported ATP-dependent uptake with half saturation at $0.4 - 0.5 \mu M$ $[Ca^{2+}]_i$ and a Hill coefficient of $1.3 - 1.7$ [22,100–102]. PMCA is described by a Hill equation with a half saturation at $0.5 \, mM$ $[Ca^{2+}]_i$ and a Hill coefficient of 2.

Cell and tissue modeling: simulations of APs, $[Ca^{2+}]_i$ and force

Our ability to integrate the information obtained from the above biophysically detailed models of individual ionic fluxes into simulations of APs and the ensuring changes in $[Ca^{2+}]_i$ and force at a cellular/tissue level were assessed by the following validations.

Model validation 1: simulation of different myometrial action potential configurations

Myometrial cells can produce different forms of APs including those consisting of a single spike, a burst of spikes or a plateau-type. A first task of validation was to assess if integration of our individual ionic current models and $[Ca^{2+}]_i$ fluxes could simulate these different AP forms.

We began to assemble a model of AP configuration that incorporated all of the currents and ion fluxes described above. However, under physiological conditions of ionic concentrations [32], this model configuration produced a resting membrane potential (RMP) that was too depolarized ($-19 \, mV$) and a basal $[Ca^{2+}]_i$ that was too high ($610 \, nM$). Many of the ionic currents described above were found in only a subset of the studied myometrial smooth muscle cells. In particular, I_{Na} was reported in only 2/30 myometrial cells in Miyoshi *et al.*, [27]. Removing I_{Na} from the model, therefore, produced an RMP of $-54 \, mV$ with a resting $[Ca^{2+}]_i$ of $116 \, nM$. When some I_{Na} is included ($\bar{g}_{Na} < 0.078 \, nS \, pF^{-1}$), the USMC model became more excitable with lower voltage threshold ($\approx -42 \, mV$) and current threshold ($\approx -0.48 \, pA \, pF^{-1}$, $20 \, ms$ stimulus). The parameters and initial conditions of the USMC model configuration are given in Table S3, S4.

The USMC model is excitable and responds to a brief stimulus with an all-or-none AP. The voltage threshold is $\approx -35 \, mV$; the corresponding current threshold is $\approx -1.05 \, pA \, pF^{-1}$ by a $20 \, ms$ stimulus. The simulated AP usually overshoots $0 \, mV$ with a maximum rate of rise (dV/dt) up to $\approx 4.8 \, V \, s^{-1}$ and the AP duration (APD) measured at $-20 \, mV$ ranges between $40 - 45 \, ms$, similar to the experimental values of dV/dt [37] and APD [100] for rodent myometrium.

The range of AP shapes reported for the pregnant rat myometrium at $30 - 35°C$ – repetitive spike AP [10], repetitive spike AP upon a depolarized basal membrane potential [101], repetitive spike AP leading to plateau [102] and a plateau-like AP [10] – are reconstructed in Figure 11. The variety of action potential shapes can be produced by this model with small variations in parameter sets and initial conditions. Of the four AP configurations illustrated in Figure 11: a bursting type AP was simulated with a current clamp of $-0.3 \, pA \, pF^{-1}$ and with the conductance of I_{Na} at $\bar{g}_{Na} = 0.12 \, nS \, pF^{-1}$; a bursting type AP upon a depolarized V was simulated with a current clamp of $-0.4 \, pA \, pF^{-1}$ and with a slope factor of $5.5 \, mV$ for the I_{CaL} inactivation steady-state; a mixed bursting-plateau type AP was simulated with $[K^+]_o$ stepped from 6 to $10 \, mM$; a plateau type AP was simulated with a current clamp of $-1.2 \, pA \, pF^{-1}$. Thus the integrated model can accommodate a variety of APs seen in uterine in smooth muscle cells.

Model validation 2: simulation of the experimental changes induced by estradiol on myometrial AP and $[Ca^{2+}]_i$ configurations

The cell model is validated with voltage-clamp and current-clamp experimental data from pregnant rat myometrial cells at $30 - 35°C$ [11,30,32,49] under control conditions and upon exposure to estradiol (Figure 12). Estradiol has been reported to reduce peak I_{CaL}. Estradiol has also been reported to reduce whole cell potassium currents [30,32,49] and change the USMC AP configuration from a bursting type AP upon a depolarized V to a plateau type AP [11]. The model was able to simulate this change in AP form by adjusting the appropriate current parameters: left-shifting the half-inactivation of I_{CaL} to $-45 \, mV$ and alters its slope factor to $10 \, mV$, and reducing total potassium conductance by 40% (Figure S1).

Model validation 3: simulation of simultaneous recordings of membrane potential, $[Ca^{2+}]_i$ and force

The extraction of the mathematical descriptions for modeling calcium-dependent force changes is denoted in Figure S6 and the resultant equations listed in the Methods (equations 3 and 8–9) and Appendix S1 (equations 104–105).

A final step in our validation of the model was to establish if it was able to accommodate the integration of uterine smooth muscle electrical, Ca^{2+} and contractile events necessary for excitation-contraction coupling. In this regard two broad scenarios of E-C coupling were again considered whereupon contractile events arose from either repetitive spike APs or from plateau-type APs. Figure 13 shows the results of simulations of APs, $[Ca^{2+}]_i$ and force compared to published experimental measurements of these variables from rat myometrial tissue at $30°C$ [103,104]. Of note, we chose to reproduce the repetitive spike AP data with four separate consequent stimuli for two reasons. First, the present USMC model, when induced by a current clamp, exhibited a lower limit for bursting frequency at $\approx 0.7 \, Hz$ which was faster than that of the experimental recordings. Second, the experimental measurements of relative membrane potential changes from Burdyga *et al.*, [103,104] were averaged from bundles of myometrial muscle strips. Thus, the low bursting frequency of spikes observed from these data may be a result of the extra electro-potential load from the multicellular environment. Alternatively, one cannot completely rule out the possibility that the four consecutive APs spikes were separate events resulting re-entrant excitation waves.

The model could also reproduce several additional published E-C coupling datasets of V(t), $[Ca^{2+}]_i(t)$ and force recorded from pregnant rats at $30 - 35°C$ [103–106] Figure S7, S8.

Limitations and Conclusions

Our approach has resulted in a number of advances for our understanding of uterine smooth muscle E-C coupling. The model encompasses the most comprehensive biophysical description of ion channel and exchanger electric currents applied to the myometrium with 14 separate electrogenic components, summarized in Figure 14, used to simulate published myometrial AP forms and their alteration by specific experimental manoeuvres. Using 105 mathematical equations, it is the first model to integrate these electrogenic components with descriptions of Ca^{2+} dynamics and phasic force production, the three essential components of electrical E-C coupling, and replicate published myometrial experimental recordings of simultaneous membrane potential, Ca^{2+} and force.

As with any mathematical model of biological phenomena there are limitations. The 14 electrogenic currents are likely to be an
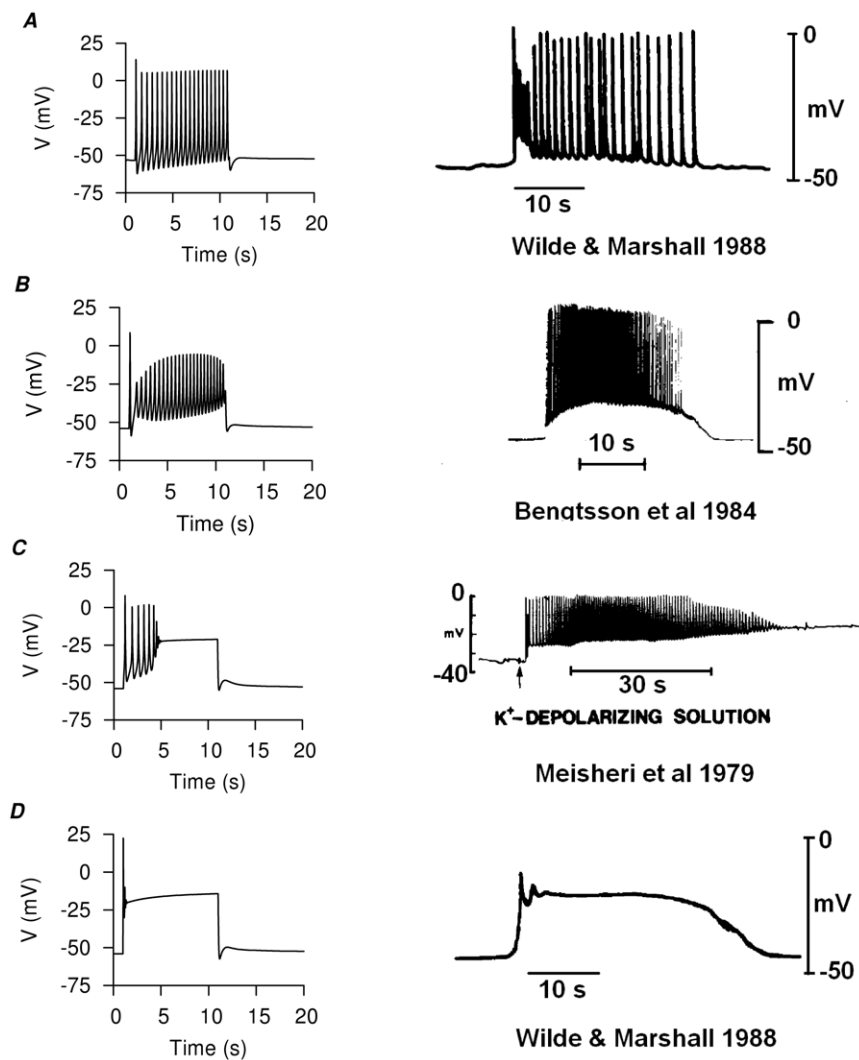
Figure 11. Varieties of action potentials. The USMC model can produce a range of myometrial action potentials (APs) using different initial conditions and parameters values. Four examples are shown (*left*); all four simulated APs were induced by a $10\,s$ stimulus applied at $t=1\,s$. Representative experimental APs from published recordings [10,101,102] are shown for comparison (*right*). A, bursting type AP with afterpotentials at resting membrane potential (RMP); B, bursting type AP with depolarized afterpotentials; C, a mixed bursting-plateau type AP with initial repetitive spikes that gradually become a flat plateau at $\approx -20\,mV$. D, plateau type AP.
doi:10.1371/journal.pone.0018685.g011

underestimate of the number of ion channel contributors to myometrial AP form. This highlights a lack of sufficient biophysical detail on other currents. In biophysical modeling of cells and tissues, it is often the case that some published electrophysiological information on particular currents is of insufficient detail to furnish biophysical modeling of all its steady-state and dynamic characteristics. Therefore, data from different resources with close cell types, or the same type of cells from different species, are used. This is the same case for the present model. The model is a hybrid containing information primarily from rat myometrium but also from human myometrium and cells expressing smooth muscle ion channel subunits, and this data has been obtained from experiments using different *in vitro* solutions and at different temperatures. Although this neglects any species-specific quantitative differences in uterine electrogenicity and E-C coupling, it presently is unavoidable. It is also common in biophysical modeling approaches when it is rare that all information is available for one cell type from one species. However, an advantage of the comprehensive assembly of this

mathematical model is that it enables identification of gaps in our knowledge of myometrial electrogenesis. This will inform future empirical work in several ways.

First, the putative contribution of many ion channel subtypes to myometrial function has often been extrapolated from molecular data (mRNA or protein) which is incomplete (not all isotypes of channel or exchanger sub-families have been examined) or pharmacological data utilizing compounds of weak specificity (*e.g.* there are many putative pharmacological blockers/openers K^+ channel sub-family that have not yet been examined on uterine function). In addition, electrophysiological isolation of currents is often lacking. Clearly, identification of the molecular expression patterns of all ion channel and ion exchanger subtypes in myometrial cells of the uterus is essential (e.g. [107]), and marrying such data to precise electrophysiological, pharmacological and simulated profiles (even if initially this is in clonal cells), is required to furnish a complete biophysical characterization of normal uterine function. This should be accomplished for rodent and human myometrium to enable one to move from the present
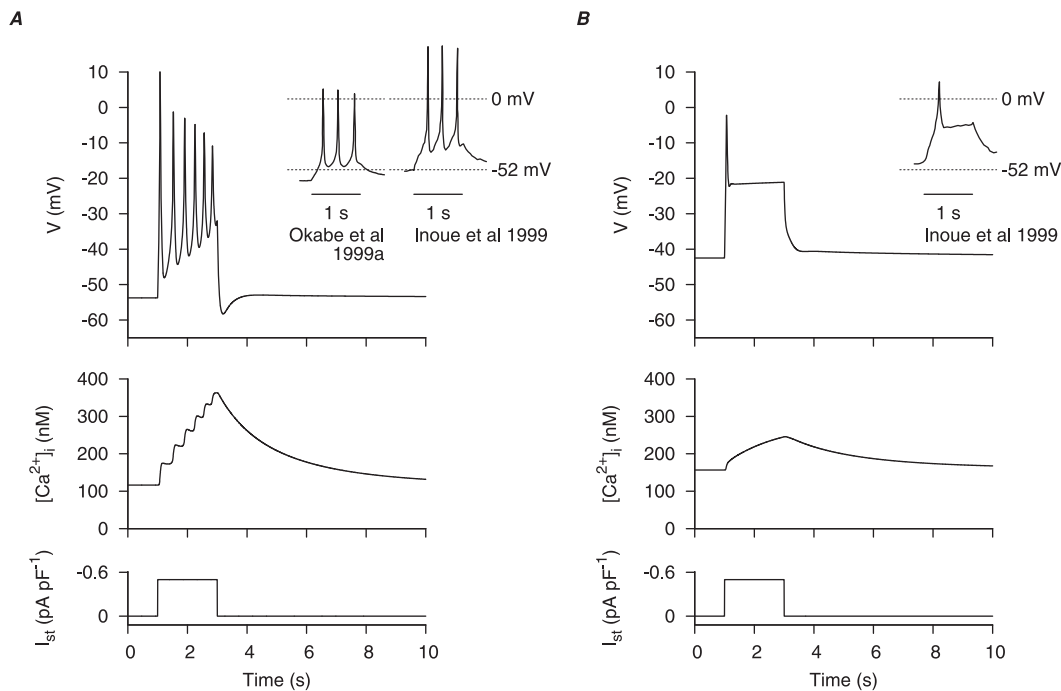
Figure 12. Simulating estradiol effects on simultaneous recordings of V and $[Ca^{2+}]_i$. Action potentials ($V(t)$) and corresponding calcium transients ($[Ca^{2+}]_i(t)$) during a 2 s depolarizing current clamp (I_{st}) under, A, control conditions and, B, the effects of estradiol. In both cases, the initial conditions of the cell model were at their corresponding numerical equilibrium. Action potentials in rat longitudinal myometrial single cells under similar experimental conditions [11,49] are shown for comparison (insets).
doi:10.1371/journal.pone.0018685.g012

hybrid model to species-specific formulations. Procedures outlined in the development of this mathematical model indicate how this can assist in improving our understanding of uterine E-C coupling.

Second, from the present information, it is clear that isolated myometrial cells exhibit heterogeneity in ion channel electrophysiology and Ca^{2+} handling characteristics (for example, the proportion of examined cells exhibiting I_{Na} or particular I_K currents). It will be important as one moves forward to consider spatiotemporal aspects of E-C coupling that we establish the implications of this for tissue level electrogenesis [5,108].

Third, the model serves as a useful tool in the design and assessment of agents that act as putative channel/exchanger blockers or activators. Refinement of the model with continued empirical/theoretical iterations will serve to increase its predictive capacity for use in the *in silico* assessment of new uterotonic agents especially as species-specific models are developed. For example, if electrophysiological data of sufficient detail for biophysical modeling is known for the actions of a new agonist/antagonist of a particular uterine ion channel then one can develop predictions of the likely action of this drug on uterine E-C coupling for that species. These will serve as hypotheses to be tested in *ex vivo* or *in vivo* experimentation. In the longer term, this should bring attendant benefits to developing drugs for the treatment of aberrant uterine activity such as preterm labor, whether experimentally induced in rodents [109] or arising spontaneously in humans, prolonged dysfunctional labor or poorly contracting uterus post-partum.

Methods

Overview

A mathematical model of uterine smooth muscle cell (USMC) function at late pregnancy was developed from the integration of

data of individual ionic currents, calcium dynamics and contraction. A glossary of symbols used in the equations is given in Table S1. The USMC model is a system of first-order ordinary differential equations,

$$dV/dt = -\sum I_{tot}/C_m \qquad (1)$$

$$d[Ca^{2+}]_i/dt = -\sum J \qquad (2)$$

$$dForce/dt = f([Ca^{2+}]_i) \qquad (3)$$

where C_m is the specific membrane capacitance. Eq. 1 describes the electrophysiological activities of myometrial membrane potential (V), which is proportional to the sum of membrane ionic currents (I_{tot}); Eq. 2 describes the corresponding intracellular calcium ($[Ca^{2+}]_i$) dynamics, which is proportional to the sum of calcium fluxes (J). Eq. 3 describes the rate of change of force as a function of $[Ca^{2+}]_i$.

Electrophysiology

The individual membrane current components that were modeled were (i) four inward currents: L-type and T-type Ca^{2+} currents (I_{CaL}, I_{CaT}), a fast inward Na^+ current (I_{Na}) and a hyperpolarization-activated current (I_h); (ii) five outward currents: two voltage-gated K^+ currents (I_{K1}, I_{K2}), an A-type transient K^+ current (I_{Ka}) and two Ca^{2+}-activated K^+ currents ($I_{K(Ca),a}$, $I_{K(Ca),ab1}$); (iii) a non-specific cation current (I_{NSCC}); (iv) a Ca^{2+}-activated Cl^- current ($I_{Cl(Ca)}$); (v) a small background potassium current (I_b); and (vi) an electrogenic Na^+-K^+ pump (I_{NaK}) and a

A

Burdyga et al 2007

B

Burdyga et al 2007

C

Mankouri et al 1998
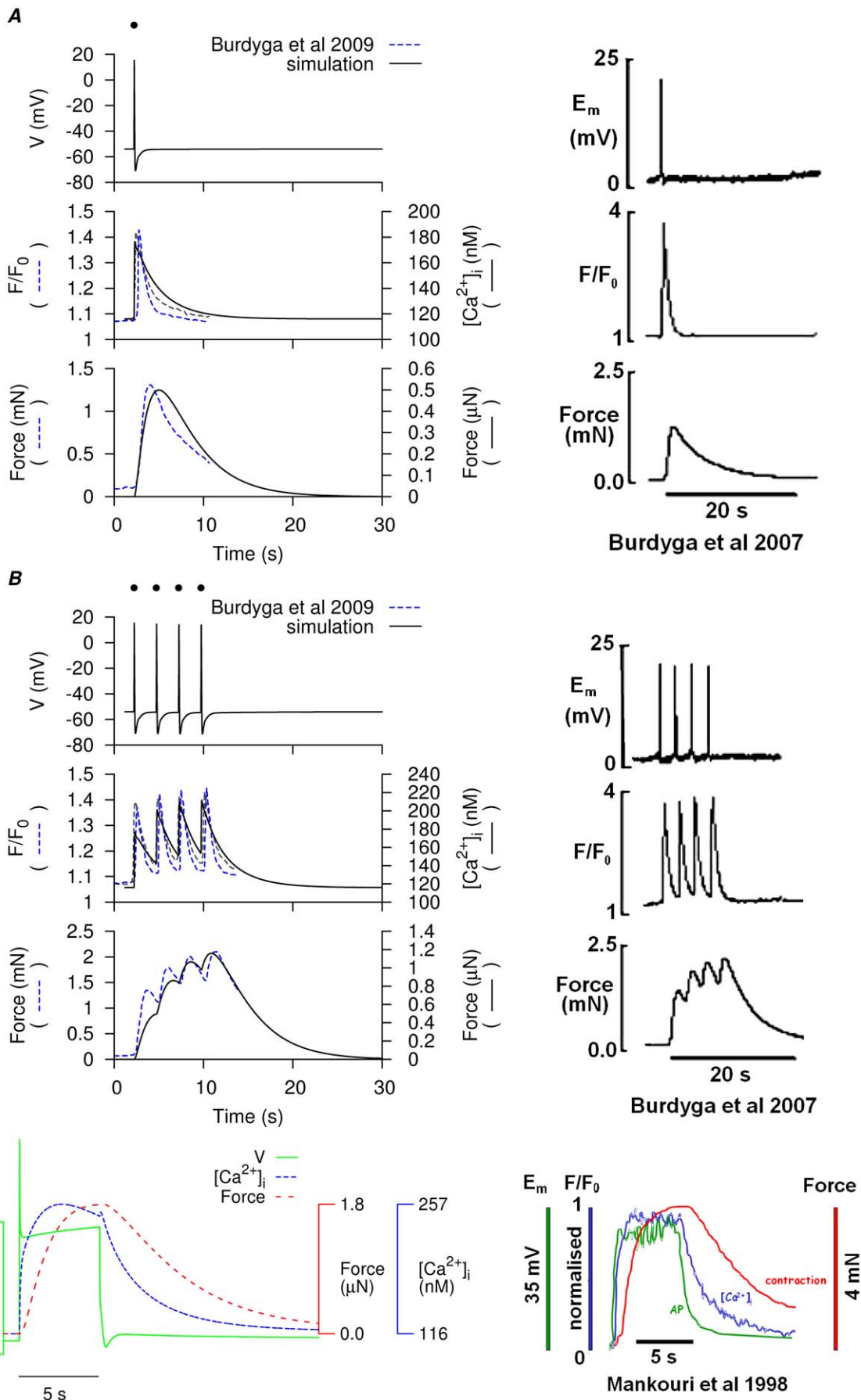
Figure 13. Simulation of the simultaneous recordings of myometrial V, $[Ca^{2+}]_i$ and force development. Simulated APs and corresponding $[Ca^{2+}]_i$ and force (*left*) compared to experimental simultaneous measurements of membrane potential, $[Ca^{2+}]_i$ and force in rat myometrial tissue strips. A, simulation of a single spike AP and corresponding $[Ca^{2+}]_i$ and force induced by a $20\,ms$ stimulus (*dot*) at $-1.5\,pA\,pF^{-1}$ and compared to experimental data [103,104]. B, four consecutive single spike APs and corresponding $[Ca^{2+}]_i$ and force modeled by $-1.5\,pA\,pF^{-1}$ stimuli (*dots*) of $20\,ms$, applied at $0.4\,Hz$ and compared to experimental data [103,104]. C, superimposed simulated AP, $[Ca^{2+}]_i$ and force development (*left*), with a $5\,s$ current clamp at $-5\,pA\,pF^{-1}$ and compared to experimental data [106].
doi:10.1371/journal.pone.0018685.g013

Na^+-Ca^{2+} exchanger (I_{NaCa}). Properties of these currents are developed based on published voltage- and current-clamp experimental data of, wherever possible, late pregnant rat myometrial cells and tissues in the literature; where rat myometrial data is not available, but complementary data is available, *e.g.*, from human USMC, or clonal cells expressing rat-derived proteins, then this has been mentioned.

Most of the membrane currents were modeled with Hodgkin-Huxley type formulation in the following form:

$$I = \bar{g}y(V - E_{rev}) \qquad (4)$$

$$E_{rev} = (RT/F)\ln([X]_o/[X]_i) \qquad (5)$$

$$dy/dt = (y_\infty - y)/\tau_y \qquad (6)$$

where $\bar{g}$ is maximum conductance, E_{rev} is the reversal potential, R is the universal gas constant, F is the Faraday constant, T is absolute temperature and $[X]_o$ and $[X]_i$ are the extracellular and intracellular ionic concentrations of ion X. The dimensionless gating variable (y) describes the time-dependent activation or inactivation profile of the channel conductance where y_∞, the steady-state value, and τ_y, the time constant, are functions of voltage and/or ionic concentrations. For the electrogenic I_{NaK} and I_{NaCa}, we adopted the formulations used in the description of cardiac ventricular cells from Nakao & Gadsby [87] and Weber *et al.*, [91] respectively. The nomenclature for the dynamic gating variables of individual membrane currents is listed in Table S2. Experimental data at body temperature, or a reported Q_{10} for an individual current, was available for I_{CaL}, I_h, $I_{Cl(Ca)}$, I_{NaK} and I_{NaCa}. For other currents, we had to assume the simplest case whereby the dynamics were similar at both room and body temperature.

Calcium dynamics

Bursztyn *et al.*, [24] modeled $[Ca^{2+}]_i$ dynamics with three major calcium fluxes in myometrial cells: membrane calcium channels ($J_{Ca,mem}$), Na^+-Ca^{2+} exchanger (J_{NaCa}) and plasma membrane Ca^{2+} ATPase (J_{PMCA}) assuming $J_{Ca,mem}$ was at its equilibrium, *i.e.*, time-independent. Herein we have included the temporal dynamics of membrane calcium currents in $J_{Ca,mem}$, and adopted the Weber *et al.*, [91] formula for Na^+-Ca^{2+} exchanger.

$J_{Ca,mem}$, which includes all the membrane calcium currents: I_{CaL}, I_{CaT} and the calcium component of I_{NSCC} ($I_{NSCC,Ca}$), was calculated from the total membrane calcium current by

$$J_{Ca,mem} = C_m A_c \beta (I_{CaL} + I_{CaL} + I_{NSCC,Ca})/(z_{Ca}FV_c) \qquad (7)$$

where C_m is the specific membrane capacitance; F is the Faraday constant; z_{Ca} is the valency of Ca^{2+} ions; A_c is the cell membrane surface area; V_c is cell volume; and β is the proportion of free intracellular Ca^{2+} ions.

The geometry of a uterine smooth muscle cell is assumed to be two cone shapes joined end-to-end at their bases [110]. Reported cell sizes for late pregnant myometrial cells are $100-300\,\mu m$ in length with a radius of $10-20\,\mu m$ [29,33]. As these dimensions cover a wide range, we represented the cell geometry with a single parameter, A_c/V_c, the surface area to volume ratio. We did not model cytoplasmic Ca^{2+} buffering proteins or intracellular calcium stores because such information for myometrial cells is too scant. Instead we assumed simply a tiny fraction of the membrane calcium influx to be free ions and the quantity is represented by the parameter β [111].

Contractile mechanism

Force development during uterine contraction was modeled with a simple first-order ordinary differential equation:

$$Force = maxForce\,\omega \qquad (8)$$
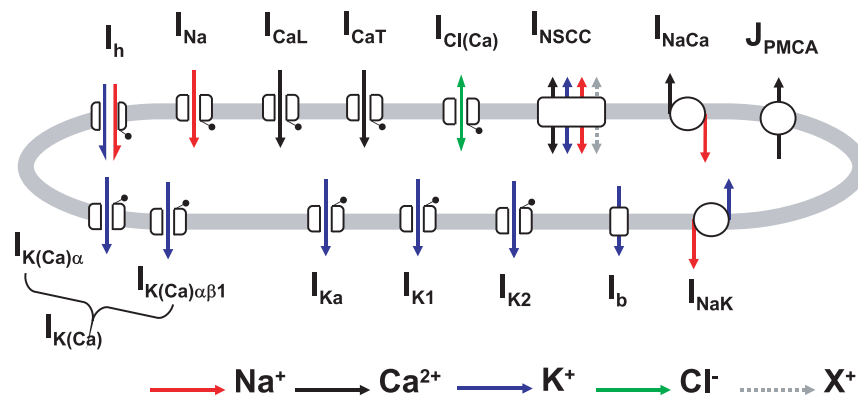
Figure 14. Schematic of the electrogenic components considered for the model of myometrial cell electrical excitability.
doi:10.1371/journal.pone.0018685.g014

$$d\omega/dt = (\omega_\infty - \omega)/\tau_\omega \qquad (9)$$

where ω is the dimensionless gating variable describing the time-dependent activation profile of force, ω_∞ the steady-state value, and τ_ω the time constant, are functions of $[Ca^{2+}]_i$. The force steady-state is described by the Ca^{2+}-activated active force relationship from non-pregnant rat myometrium at $20-22°C$ [112]; the time constant function is chosen to reproduce force development in late pregnant myometrial tissues recorded at $30-33°C$ [103,104] (Figure S6).

Model simulations

Action potentials were induced in the whole cell model by applying an external stimulus current (I_{st}), either as brief square pulses for single spike AP or with a current clamp for bursting or plateau AP.

The initial values of the dynamical variables (V, $[Ca^{2+}]_i$, membrane current gating variables, and ω) are listed in Table S3. The parameter values, which remain constant during simulations, are listed in Table S4. All the equations are given in Appendix S1.

Simulations were computed with a fixed time step of $0.02\,ms$, using XPPAUT [113] with either the fourth-order Runge-Kutta numerical integration method or the Euler Method, in a IBM laptop PC with a Intel(R) Pentium(R) M 1.5 GHz single processor. The Runge-Kutta was the method of choice for developing individual components and short simulations of the whole cell model whereas the Euler method was mainly used for simulations requiring longer integration times. Solutions of the whole USMC model using both integration methods are almost identical.

A copy of the model source code written in the C programming language is included in Appendix S2.

Annotation of Figures

Within the body of some Figures there are textual annotations that mention the source references for the data plotted in those diagrams. Those references without parenthesis indicate published values that we have reproduced in the diagram. The references mentioned within parentheses reflect data that we have extracted from published raw tracings and refitted as displayed in the figures. Data referred to as 'unpublished' is remarked upon in the main text.

Supporting Information

Figure S1 Simulating the effect of estradiol on the inactivation of myometrial I_{CaL}.
(PDF)

Figure S2 Different inactivation kinetics of myometrial $I_{CaT}s$.
(PDF)

Figure S3 Divalent ion concentration versus I_{CaT} inactivation time constant of rat myometrial I_{CaT}.
(PDF)

Figure S4 Experimental current tracings of I_{K1} from five cells and an example of extrapolated I_{K1} at the voltage step (V_s) $+10\,mV$ averaged from these five cells.
(PDF)

Figure S5 Experimental current tracings of I_{K2} from four cells and an example of extrapolated I_{K2} at the voltage step (V_s) $+10\,mV$ averaged from these four cells.
(PDF)

Figure S6 Modeling the dynamics of $[Ca^{2+}]_i$-dependent active force.
(PDF)

Figure S7 Modeling simultaneous changes in V and $[Ca^{2+}]_i$ or $[Ca^{2+}]_i$ and force development.
(PDF)

Figure S8 Modeling force output consequent to spike APs or plateau-like APs.
(PDF)

Table S1 Definitions of the equation symbols.
(PDF)

Table S2 Definition of gating variables for individual currents and force, and the corresponding experimental temperature and species.
(PDF)

Table S3 Initial values of the dynamics variables used in model simulations.
(PDF)

Table S4 Constant parameter values used in model simulations.
(PDF)

Appendix S1 Equations used in the model simulations.
(PDF)

Appendix S2 Model source code.
(BZ2)

Acknowledgments

Author Contributions

Conceived and designed the experiments: MJT HZ AVH. Performed the experiments: WCT CYC SK. Analyzed the data: MJT HZ AVH WCT. Contributed reagents/materials/analysis tools: MJT HZ AVH WCT. Wrote the paper: MJT HZ WCT.

References

1. Landa J, West TC (1956) Transmembrane potentials and contractility in the pregnant rat uterus. Am J Physiol 187: 333–337.
2. Landa JF, West TC, Thiersch JB (1959) Relationships between contraction and membrane electrical activity in the isolated uterus of the pregnant rat. Am J Physiol 196: 905–909.
3. Csapo IA, Kuriyama HA (1963) Effects of ions and drugs on cell membrane activity and tension in the postpartum rat myometrium. J Physiol 165: 575–592.
4. Garfield RE, Maner WL (2007) Physiology and electrical activity of uterine contractions. Semin Cell Dev Biol 18: 289–295.
5. Taggart MJ, Morgan KG (2007) Regulation of the uterine contractile apparatus and cytoskeleton. Semin Cell Dev Biol 18: 296–304.
6. Goldenberg RL, Culhane JF, Iams JD, Romero R (2008) Epidemiology and causes of preterm birth. Lancet 371: 75–84.
7. Bugg GJ, Stanley E, Baker PN, Taggart MJ, Johnston TA (2006) Outcomes of labours augmented with oxytocin. Eur J Obstet Gynecol Reprod Biol 124: 37–41.
8. Parkington HC, Tonta MA, Davies NK, Brennecke SP, Coleman HA (1999) Hyperpolarization and slowing of the rate of contraction in human uterus in pregnancy by prostaglandins E_2 and $F_{2\alpha}$: Involvement of the Na^+ pump. J Physiol 514(Pt 1): 229–243.
9. Taggart MJ, Tribe RM (2007) Cellular ionic mechanisms controlling uterine smooth muscle contraction: effects of gestational state. In: Savinneau JP, ed. New Frontiers in Smooth Muscle Biology and Physiology. , India: Research Signpost. pp 523–549. ISBN: 9788178952956.
10. Wilde DW, Marshall JM (1988) Effects of tetraethylammonium and 4-aminopyridine on the plateau potential of circular myometrium from the pregnant rat. Biol Reprod 38: 836–845.

11. Inoue Y, Okabe K, Soeda H (1999) Augmentation and suppression of action potentials by estradiol in the myometrium of pregnant rat. Can J Physiol Pharmacol 77: 447–453.

12. Shmigol AV, Eisner DA, Wray S (1998) Properties of voltage-activated $[Ca^{2+}]_i$ transients in, single smooth muscle cells isolated from pregnant rat uterus. J Physiol 511: 803–811.

13. Blanks AM, Zhao ZH, Shmygol A, Bru-Mercier G, Astle S, et al. (2007) Characterization of the molecular and electrophysiological properties of the T-type calcium channel in human myometrium. J Physiol 581: 915–926.

14. Sperelakis N, Inoue Y, Ohya Y (1992) Fast Na^+ channels and slow Ca^{2+} current in smooth muscle from pregnant rat uterus. Mol Cell Biochem 114: 79–89.

15. Jones K, Shmygol A, Kupittayanant S, Wray S (2004) Electrophysiological characterization and functional importance of calcium-activated chloride channel in rat uterine myocytes. Pflugers Arch 448: 36–43.

16. Khan RN, Smith SK, Morrison JJ, Ashford ML (1993) Properties of large-conductance K^+ channels in human myometrium during pregnancy and labour. Proc Biol Sci 251: 9–15.

17. Wang SY, Yoshino M, Sui JL, Wakui M, Kao PN, et al. (1998) Potassium currents in freshly dissociated uterine myocytes from nonpregnant and late-pregnant rats. J Gen Physiol 112: 737–756.

18. Knock GA, Aaronson PI (1999) Calcium antagonistic properties of the cyclooxygenase-2 inhibitor nimesulide in human myometrial myocytes. Br J Pharmacol 127: 1470–1478.

19. Knock GA, Smirnov SV, Aaronson PI (1999) Voltage-gated K^+ currents in freshly isolated myocytes of, the pregnant human myometrium. J Physiol 518: 769–781.

20. Noble K, Floyd R, Shmygol A, Shmygol A, Mobasheri A, et al. (2010) Distribution, expression and functional effects of small conductance Ca-activated potassium (SK) channels in rat myometrium. Cell Calcium 47: 47–54.

21. Floyd RV, Wray S, Quenby S, Martin-Vasallo P, Mobasheri A (2010) Expression and distribution of Na, K-ATPase isoforms in the human uterus. Reprod Sci 17: 366–376.

22. Grover AK, Kwan CY, Daniel EE (1981) Na-Ca exchange in rat myometrium membrane vesicles highly enriched in plasma membranes. Am J Physiol 240: C175–82.

23. Taggart MJ, Blanks A, Kharche S, Holden A, Wang B, et al. (2007) Towards understanding the myometrial physiome: approaches for the construction of a virtual physiological uterus. BMC Pregnancy Childbirth 7 Suppl 1: S3.

24. Bursztyn L, Eytan O, Jaffa AJ, Elad D (2007) Mathematical model of excitation-contraction in a uterine smooth muscle cell. Am J Physiol cell Physiol 292: 1816–1829.

25. Rihana S, Terrien J, Germain G, Marque C (2009) Mathematical modeling of electrical activity of uterine muscle cells. Med Biol Eng Comput 47: 665–675.

26. Jmari K, Mironneau C, Mironneau J (1986) Inactivation of calcium channel current in rat uterine smooth muscle: evidence for calcium- and voltage-mediated mechanisms. J Physiol 380: 111–126.

27. Miyoshi H, Urabe T, Fujiwara A (1991) Electrophysiological properties of membrane currents in single myometrial, cells isolated from pregnant rats. Pflugers Arch 419: 386–393.

28. Young RC, Smith LH, McLaren MD (1993) T-type and L-type calcium currents in freshly dispersed human uterine smooth muscle cells. Am J Obstet Gynecol 169: 785–792.

29. Amedee T, Mironneau C, Mironneau J (1987) The calcium channel current of pregnant rat single myometrial cells, in short-term primary culture. J Physiol 392: 253–272.

30. Yamamoto T (1995) Effects of estrogens on Ca channels in myometrial cells isolated from pregnant rats. Am J Physiol 268: C64–9.

31. Mcdonald TF, Pelzer S, Trautwein W, Pelzer DJ (1994) Regulation and modulation of calcium channels in cardiac, skeletal, and smooth muscle. Physiol Rev 74: 365–507.

32. Okabe K, Inoue Y, Soeda H (1999) Estradiol inhibits Ca^{2+} and K^+ channels in smooth muscle cells from pregnant rat myometrium. Eur J Pharmacol 376: 101–108.

33. Yoshino M, Wang SY, Kao CY (1997) Sodium and calcium inward currents in freshly dissociated smooth myocytes of rat uterus. J Gen Physiol 110: 565–577.

34. Inoue Y, Sperelakis N (1991) Gestational change in Na^+ and Ca^{2+} channel current densities, in rat myometrial smooth muscle cells. Am J Physiol 260: C658–63.

35. Kusaka M, Sperelakis N (1995) Inhibition of L-type calcium current by genistein, a tyrosine kinase inhibitor, in pregnant rat myometrial cells. Biochim Biophys Acta 1240: 196–200.

36. Greenwood IA, Large WA (1996) Analysis of the time course of calcium-activated chloride 'tail' currents in rabbit portal vein smooth muscle cells. Pflugers Arch 432: 970–979.

37. Parkington HC, Coleman HA (2001) Excitability in uterine smooth muscle. Front Horm Res 27: 179–200.

38. Mershon JL, Mikala G, Schwartz A (1994) Changes in the expression of the L-type voltage-dependent calcium channel during pregnancy and parturition in the rat. Biol Reprod 51: 993–1002.

39. Tezuka N, Ali M, Chwalisz K, Garfield RE (1995) Changes in transcripts encoding calcium channel subunits of rat myometrium during pregnancy. Am J Physiol 269: C1008–17.

40. Ohkubo T, Kawarabayashi T, Inoue Y, Kitamura K (2005) Differential expression of L- and T-type calcium channels between, longitudinal and circular muscles of the rat myometrium during pregnancy. Gynecol Obstet Invest 59: 80–85.

41. Helguera G, Olcese R, Song M, Toro L, Stefani E (2002) Tissue-specific regulation of Ca^{2+} channel protein expression by sex hormones. Biochim Biophys Acta 1569: 59–66.

42. Ohya Y, Sperelakis N (1989) Fast Na^+ and slow Ca^{2+} channels in single uterine muscle cells from pregnant rats. Am J Physiol 257: C408–12.

43. Serrano JR, Perez-Reyes E, Jones SW (1999) State-dependent inactivation of the alpha1G T-type calcium channel. J Gen Physiol 114: 185–201.

44. Hering J, Feltz A, Lambert RC (2003) Slow inactivation of the Cav3.1 isotype of T-type calcium channels. J Physiol 555: 331–344.

45. Asokan KT, Sarkar SN, Mishra SK, Raviprakash V (2002) Effects of mibefradil on uterine contractility. Eur J Pharmacol 455: 65–71.

46. Lee SE, Ahn DS, Lee YH (2009) Role of T-type Ca channels in the spontaneous phasic contraction of pregnant rat uterine smooth muscle. Korean J Physiol Pharmacol 13: 241–249.

47. Inoue Y, Nakao K, Okabe K, Izumi H, Kanda S, et al. (1990) Some electrical properties of human pregnant myometrium. Am J Obstet Gynecol 162: 1090–1098.

48. Satoh H (1995) Identification of a hyperpolarization-activated inward current in uterine smooth muscle cells during pregnancy. Gen Pharmacol 26: 1335–1338.

49. Okabe K, Inoue Y, Kawarabayashi T, Kajiya H, Okamoto F, et al. (1999) Physiological significance of hyperpolarization-activated inward currents (ih) in smooth muscle cells from the circular layers of pregnant rat myometrium. Pflugers Arch 439: 76–85.

50. Shannon TR, Wang F, Puglisi J, Weber C, Bers DM (2004) A mathematical treatment of integrated Ca dynamics within the ventricular myocyte. Biophys J 87: 3351–3371.

51. Knock GA, Tribe RM, Hassoni AA, Aaronson PI (2001) Modulation of potassium current characteristics in human myometrial smooth muscle by 17beta-estradiol and progesterone. Biol Reprod 64: 1526–1534.

52. Erulkar SD, Rendt J, Nori RD, Ger B (1994) The influence of 17 beta-oestradiol on K^+ currents in smooth muscle cells isolated from immature rat uterus. Proc Biol Sci 256: 59–65.

53. Piedras-Renteria E, Stefani E, Toro L (1991) Potassium currents in freshly dispersed myometrial cells. Am J Physiol 261: C278–84.

54. Anwer K, Toro L, Oberti C, Stefani E, Sanborn BM (1992) Ca^{2+}-activated K^+ channels in pregnant rat myometrium: modulation by a beta-adrenergic agent. Am J Physiol 263: C1049–56.

55. Anwer K, Oberti C, Perez GJ, Perez-Reyes N, Mcdougall JK, et al. (1993) Calcium-activated K^+ channels as modulators of human myometrial contractile activity. Am J Physiol 265: C976–85.

56. Perez GJ, Toro L, Erulkar SD, Stefani E (1993) Characterization of large-conductance, calcium-activated potassium channels from human myometrium. Am J Obstet Gynecol 168: 652–660.

57. Song M, Zhu N, Olcese R, Barila B, Toro L, et al. (1999) Hormonal control of protein expression and mRNA levels of the MaxiK channel alpha subunit in myometrium. FEBS Lett 460: 427–432.

58. Zhou XB, Wang GX, Ruth P, Huneke B, Korth M (2000) BK(Ca) channel activation by membrane-associated cGMP kinase may contribute to uterine quiescence in pregnancy. Am J Physiol Cell Physiol 279: C1751–9.

59. Matharoo-Ball B, Ashford MLJ, Arulkumaran S, Khan RN (2003) Down-regulation of the alpha- and beta-subunits of the calcium-activated potassium channel in human myometrium with parturition. Biol Reprod 68: 2135–2141.

60. Curley M, Morrison JJ, Smith TJ (2004) Analysis of maxi-K alpha subunit splice variants in human myometrium. Reprod Biol Endocrinol 2: 67.

61. Khan RN, Smith SK, Ashford ML (1998) Contribution of calcium-sensitive potassium channels to NS1619-induced relaxation in human pregnant myometrium. Hum Reprod 13: 208–213.

62. Khan RN, Matharoo-Ball B, Arulkumaran S, Ashford ML (2001) Potassium channels in the human myometrium. Exp Physiol 86: 255–264.

63. Bao L, Cox DH (2005) Gating and ionic currents reveal how the BK(Ca) channel's Ca^{2+} sensitivity is enhanced by its beta1 subunit. J Gen Physiol 12: 393–412.

64. Orio P, Torres Y, Rojas P, Carvacho I, Garcia ML, et al. (2006) Structural determinants for functional coupling between the beta and alpha subunits in the Ca^{2+}-activated K^+ (BK) channel. J Gen Physiol 127: 191–204.

65. Benkusky NA, Fergus DJ, Zucchero TM, England SK (2000) Regulation of the Ca^{2+}-sensitive domains of the maxi-K channel in the mouse myometrium during gestation. J Biol Chem 275: 27712–27719.

66. Zhou XB, Wang GX, Huneke B, Wieland T, Korth M (2000) Pregnancy switches adrenergic signal transduction in rat and human uterine myocytes as probed by BKCa channel activity. J Physiol 524: 339–352.

67. Shmigol A, Eisner DA, Wray S (1998) Carboxyeosin decreases the rate of decay of the $[Ca^{2+}]_i$ transient in uterine smooth muscle cells isolated from pregnant rats. Pflugers Arch 437: 158–160.

68. Brown A, Cornwell T, Korniyenko I, Solodushko V, Bond CT, et al. (2007) Myometrial expression of small conductance Ca^{2+}-activated K^+ channels depresses phasic uterine contraction. Am J Physiol Cell Physiol 292: C832–C840.

69. Smith RC, McClure MC, Smith MA, Abel PW, Bradley ME (2007) The role of voltage-gated potassium channels in the regulation of mouse uterine contractility. Reprod Biol Endocrinol 5: 41.

70. Pierce SL, Kresowik JDK, Lamping KG, England SK (2008) Overexpression of SK3 channels dampens uterine contractility to prevent preterm labor in mice. Biol Reprod 78: 1058–1063.

71. McCallum LA, Pierce SL, England SK, Greenwood IA, Tribe RM (2011) The contribution of Kv7 channels to pregnant mouse and human myometrial contractility. J Cell Mol Med 15: 577–86.

72. Coleman HA, Parkington HC (1987) Single channel Cl$^-$ and K$^+$ currents from cells of uterus not treated with enzymes. Pflugers Arch 410: 560–562.

73. Mironneau J, Arnaudeau S, Macrez-Lepretre N, Boittin FX (1996) Ca^{2+} sparks and Ca^{2+} waves activate different Ca^{2+}-dependent ion channels in single myocytes from rat portal vein. Cell Calcium 20: 153–160.

74. Young RC, Bemis A (2009) Calcium-activated chloride currents prolongs the duration of contractions in pregnant rat myometrial tissue. Reprod Sci 16: 734–739.

75. Jeong JW, Lee KY, Lydon JP, DeMayo FJ (2006) Steroid hormone regulation of Clca3 expression in the murine uterus. J Endocrinol 189: 473–484.

76. Song J, Zhang X, Qi Z, Sun G, Chi S, et al. (2009) Cloning and characterization of a calcium-activated chloride channel in rat uterus. Biol Reprod 80: 788–794.

77. Arreola J, Melvin JE, Begenisich T (1996) Activation of calcium-dependent chloride channels in rat parotid acinar cells. J Gen Physiol 108: 35–47.

78. Angermann JE, Sanguinetti AR, Kenyon JL, Leblanc N, Greenwood IA (2006) Mechanism of the inhibition of Ca^{2+}-activated Cl$^-$ currents by phosphorylation in pulmonary arterial smooth muscle cells. J Gen Physiol 128: 73–87.

79. Miyoshi H, Yamaoka K, Garfield RE, Ohama K (2004) Identification of a non-selective cation channel current in myometrial cells isolated from pregnant rats. Pflugers Arch 447: 457–464.

80. Chang DC (1983) Dependence of cellular potential on ionic concentrations. data supporting a modification of the constant field equation. Biophys J 43: 149–156.

81. Manabe K, Takano M, Noma A (1995) Non-selective cation current of guinea-pig endocardial endothelial cells. J Physiol 487: 407–419.

82. Taylor GS, Paton DM, Daniel EE (1969) Evidence for an electrogenic sodium pump in smooth muscle. Life Sci 8: 769–773.

83. Taylor GS, Paton DM, Daniel EE (1970) Characteristics of electrogenic sodium pumping in rat myometrium. J Gen Physiol 56: 360–375.

84. Turi A, Marcsek Z, Mullner N, Kucsera M, Bori Z (1992) The activity of Na$^+$/K$^+$-ATPase and abundance of its mRNA are regulated in rat myometrium during pregnancy. Biochem Biophys Res Commun 188: 1191–1198.

85. Esplin MS, Fausett MB, Faux DS, Graves SW (2003) Changes in the isoforms of the sodium pump in the placenta and myometrium of women in labor. Am J Obstet Gynecol 188: 759–764.

86. Vance CJ, Esplin MS, Hamblin S, Graves SW (2006) Alterations in uterine sodium pump abundance may contribute to the onset and progression of term and preterm labor in mice. Am J Obstet Gynecol 195: 1407–1414.

87. Nakao M, Gadsby DC (1989) [Na] and [K] dependence of the Na/K pump current-voltage relationship in guinea pig ventricular myocytes. J Gen Physiol 94: 539–565.

88. Nakamura Y, Ohya Y, Abe I, Fujishima M (1999) Sodium-potassium pump current in smooth muscle cells from mesenteric resistance arteries of the guinea-pig. J Physiol 519: 203–212.

89. Taggart MJ, Wray S (1997) Agonist mobilization of sarcoplasmic reticular calcium in smooth muscle: Functional coupling to the plasmalemmal Na$^+$/Ca^{2+} exchanger? Cell Calcium 22: 333–341.

90. Shmigol AV, Eisner DA, Wray S (1999) The role of the sarcoplasmic reticulum as a Ca^{2+} sink in rat uterine smooth muscle cells. J Physiol 520 Pt 1: 153–163.

91. Weber CR, Ginsburg KS, Philipson KD, Shannon TR, Bers DM (2001) Allosteric regulation of Na/Ca exchange current by cytosolic Ca in intact cardiac myocytes. J Gen Physiol 117: 119–131.

92. Abe Y (1971) Effects of changing the ionic environment on passive and active membrane properties of pregnant rat uterus. J Physiol 214: 173–190.

93. Quednau BD, Nicoll DA, Philipson KD (1997) Tissue specificity and alternative splicing of the Na$^+$/Ca^{2+} exchanger isoforms NCX1, NCX2, and NCX3 in rat. Am J Physiol Cell Physiol 272: C1250–1261.

94. Levitsky DO (2007) Three types of muscles express three sodium-calcium exchanger isoforms. Ann NY Acad Sci 1099: 221–225.

95. Li Z, Matsuoka S, Hryshko LV, Nicoll DA, Bersohn MM, et al. (1994) Cloning of the NCX2 isoform of the plasma membrane Na$^+$-Ca^{2+} exchanger. J Biol Chem 269: 17434–17439.

96. Iwamoto T, Shigekawa M (1998) Differential inhibition of Na$^+$/Ca^{2+} exchanger isoforms by divalent cations and isothiourea derivative. Am J Physiol 275: C423–30.

97. Linck B, Qiu Z, He Z, Tong Q, Hilgemann DW, et al. (1998) Functional comparison of the three isoforms of the Na$^+$/Ca^{2+} exchanger (NCX1, NCX2, NCX3). Am J Physiol 274: C415–23.

98. Campbell DL, Giles WR, Robinson K, Shibata EF (1988) Studies of the sodium-calcium exchanger in bull-frog atrial myocytes. J Physiol 403: 317–340.

99. Vigne P, Breittmayer JP, Duval D, Frelin C, Lazdunski M (1988) The Na$^+$/Ca^{2+} antiporter in aortic smooth muscle cells. J Biol Chem 263: 8078–8083.

100. Mollard P, Mironneau J, Amedee T, Mironneau C (1986) Electrophysiological characterization of single pregnant rat myometrial cells in short-term primary culture. Am J Physiol 250: C47–54.

101. Bengtsson B, Chow EM, Marshall JM (1984) Activity of circular muscle of rat uterus at different times in pregnancy. Am J Physiol 246: C216–23.

102. Meisheri KD, Mcneill JH, Marshall JM (1979) Effect of isoproterenol on the isolated pregnant rat myometrium. Eur J Pharmacol 60: 1–6.

103. Burdyga T, Wray S, Noble K (2007) In situ calcium signaling. no calcium sparks detected in rat myometrium. Ann N Y Acad Sci 1101: 85–96.

104. Burdyga T, Borisova L, Burdyga AT, Wray S (2009) Temporal and spatial variations in spontaneous Ca events and mechanical activity in pregnant rat myometrium. Eur J Obstet Gynecol Reprod Biol 144 Suppl 1: S25–S32.

105. Kawarabayashi T (1994) Electrophysiology of the human myometrium. In: Chard T, Grudzinskas JG, eds. The Uterus. Cambridge, UK: Cambridge University Press, Cambridge Reviews in Human Reproduction, chapter 7. pp 148–172.

106. Mankouri HW, Burdyga T, Taggart MJ, Wray S (1998) Simultaneous measurements of electrical activity, intracellular calcium and contraction in smooth muscle. J Physiol 509.P: 2P–3P.

107. Zhang J, Taggart M, Thornton S, Shmygol A, Blanks AM (2010) The pregnancy dependent expression profile of the genomic complement of K channels in human myometrial smooth muscle and vasculature. Reprod Sci 17: 78A.

108. Lammers WJEP, Mirghani H, Stephen B, Dhanasekaran S, Wahab A, et al. (2008) Patterns of electrical propagation in the intact pregnant guinea pig uterus. Am J Physiol Regul Integr Comp Physiol 294: R919–R928.

109. Mitchell BF, Taggart MJ (2009) Are animal models relevant to key aspects of human parturition? Am J Physiol Regul Integr Comp Physiol 297: R525–R545.

110. Kamishima T, Mccarron JG (1996) Depolarization-evoked increases in cytosolic calcium concentration in isolated smooth muscle cells of rat portal vein. J Physiol 492(Pt 1): 61–74.

111. Standen NB, Stanfield PR (1982) A binding-site model for calcium channel inactivation that depends on calcium entry. Proc R Soc Lond B Biol Sci 217: 101–110.

112. Crichton CA, Taggart MJ, Wray S, Smith GL (1993) Effects of pH and inorganic phosphate on force production in alpha-toxin-permeabilized isolated rat uterine smooth muscle. J Physiol 465: 629–645.

113. Ermentrout GB (2002) Simulating, analyzing, and animating dynamical systems: a guide to XPPAUT for researchers and students. Philadelphia, US: Society for Industrial and Applied Mathematics.